PLOS PATHOGENS

RESEARCH ARTICLE

Proteasomal inhibition triggers viral oncoprotein degradation via autophagy-lysosomal pathway

Chandrima Gain[1], Samaresh Malik[1], Shaoni Bhattacharjee[1], Arijit Ghosh[2], Erle S. Robertson[3], Benu Brata Das[2], Abhik Saha[1]*

1 Department of Life Sciences, Presidency University, West Bengal, India, **2** Laboratory of Molecular Biology, School of Biological Sciences, Indian Association for the Cultivation of Science, Jadavpur, Kolkata, India, **3** Department of Otorhinolaryngology Head and Neck Surgery, and the Tumor Virology Program, Abramson Comprehensive Cancer Center, Perelman School of Medicine at the University of Pennsylvania, Philadelphia, Pennsylvania, United States of America

* abhik.dbs@presiuniv.ac.in

Citation: Gain C, Malik S, Bhattacharjee S, Ghosh A, Robertson ES, Das BB, et al. (2020) Proteasomal inhibition triggers viral oncoprotein degradation via autophagy-lysosomal pathway. PLoS Pathog 16(2): e1008105. https://doi.org/10.1371/journal.ppat.1008105

Editor: Robert F. Kalejta, University of Wisconsin-Madison, UNITED STATES

Received: September 15, 2019

Accepted: January 28, 2020

Published: February 24, 2020

Data Availability Statement: All relevant data are within the manuscript and its Supporting Information files.

Funding: E.S.R. is a scholar of the Leukemia and Lymphoma Society of America. A.S. and B.B.D. are Wellcome Trust/DBT India Alliance Intermediate Fellows. C.B. and S.M. are the recipients of UGC-NET Senior and Junior Research Fellowship, respectively, India. S.B. is recipient of DST-Inspire Senior Research Fellowship and A.G. is recipient of CSIR-NET Senior Research Fellowship. This work

Abstract

Epstein-Barr virus (EBV) nuclear oncoprotein EBNA3C is essential for B-cell transformation and development of several B-cell lymphomas particularly those are generated in an immuno-compromised background. EBNA3C recruits ubiquitin-proteasome machinery for deregulating multiple cellular oncoproteins and tumor suppressor proteins. Although EBNA3C is found to be ubiquitinated at its N-terminal region and interacts with 20S proteasome, the viral protein is surprisingly stable in growing B-lymphocytes. EBNA3C can also circumvent autophagy-lysosomal mediated protein degradation and subsequent antigen presentation for T-cell recognition. Recently, we have shown that EBNA3C enhances autophagy, which serve as a prerequisite for B-cell survival particularly under growth deprivation conditions. We now demonstrate that proteasomal inhibition by MG132 induces EBNA3C degradation both in EBV transformed B-lymphocytes and ectopic-expression systems. Interestingly, MG132 treatment promotes degradation of two EBNA3 family oncoproteins–EBNA3A and EBNA3C, but not the viral tumor suppressor protein EBNA3B. EBNA3C degradation induced by proteasomal inhibition is partially blocked when autophagy-lysosomal pathway is inhibited. In response to proteasomal inhibition, EBNA3C is predominantly K63-linked polyubiquitinated, colocalized with the autophagy-lysosomal fraction in the cytoplasm and participated within p62-LC3B complex, which facilitates autophagy-mediated degradation. We further show that the degradation signal is present at the first 50 residues of the N-terminal region of EBNA3C. Proteasomal inhibition reduces the colony formation ability of this important viral oncoprotein, induces apoptotic cell death and increases transcriptional activation of both latent and lytic gene expression which further promotes viral reactivation from EBV transformed B-lymphocytes. Altogether, this study offers rationale to use proteasome inhibitors as potential therapeutic strategy against multiple EBV associated B-cell lymphomas, where EBNA3C is expressed.

was supported by grants from Wellcome Trust/ DBT India Alliance Intermediate Fellowship research grant (IA/I/14/2/501537), Department of Biotechnology (DBT), Govt. of India (BT/PR8123/ MED/30/990/2013) and Department of Science and Technology (DST), Govt. of India (CRG/2018/ 001044) to A.S. The funders had no role in study design, data collection and analysis, decision to publish, or preparation of the manuscript.

Competing interests: The authors have declared that no competing interests exist.

Author summary

Epstein-Barr virus (EBV) establishes latent infection in B-lymphocytes and is associated with a number of human malignancies, both of epithelial and lymphoid origin. EBV encoded EBNA3 family of nuclear latent antigens comprising of EBNA3A, EBNA3B, and EBNA3C are unique to immunoblastic lymphomas. While EBNA3A and EBNA3C are involved in blocking many important tumor suppressive mechanisms, EBNA3B exhibits tumor suppressive functions. Although EBNA3 proteins, in particular EBNA3C, interact with and employ different protein degradation machineries to induce B-cell lymphomagenesis, these viral proteins are extremely stable in growing B-lymphocytes. To this end, we now demonstrate that proteasomal inhibition leads to specifically degradation of oncogenic EBNA3A and EBNA3C proteins, whereas EBNA3B remains unaffected. Upon proteasomal inhibition, EBNA3C degradation occurs via autophagy-lysosomal pathway, through labeling with K63-linked polyubiquitination and participating in p62-LC3B complex involved in ubiquitin-mediated autophagy substrate selection and degradation through autolysosomal process. We also demonstrate that the N-terminal domain is responsible for autophgy-lysosomal mediated degradation, while the C-terminal domain plays a crucial role in cytoplasmic localization. Fascinatingly, while proteasomal inhibition reduces EBNA3C's oncogenic property, it induces both latent and lytic gene expressions and promotes viral reactivation from EBV transformed B-lymphocytes. This is the first report which demonstrates a viral oncoprotein degrades through autophagy-lysosomal pathway upon proteasomal inhibition. In sum, the results promise development of novel strategies specifically targeting proteolytic pathway for the treatment of EBV associated B-cell lymphomas, particularly those are generated in immunocompromised individuals.

Introduction

Epstein-Barr virus (EBV) is a large DNA virus that belongs to the gammaherpesvirus subfamily and persistently infects majority of the worldwide human population [1,2,3]. In spite of being a ubiquitous virus, EBV is recognized as one of the most efficient transforming viruses and responsible for development of several neoplasms, mostly of B-cell origin, but also some epithelial origin such as nasopharyngeal, breast and gastric carcinomas. There are three major types of B-cell malignancies causally associated with EBV are the Burkitt's lymphoma (BL), Hodgkin's lymphoma (HL) and diffuse large B cell lymphomas (DLBCL) [2,4]. EBV is also detected as the etiologic factor of majority of infectious mononucleosis (IM), a lymphoproliferative disorder attributable to a striking increase in $CD8^+$ T-cell activation and subsequent expansion of B-lymphocytes upon viral infection [5]. This clinical manifestation of primary EBV infection indicates its competence not only to embark on latent infection in B-lymphocytes but also to impel B-cell proliferation *in vivo*. Moreover, *in vitro* EBV transforms nascent B-lymphocytes into continuously proliferating lymphoblastoid cell lines (LCLs) with phenotypic resemblance of activated B-blasts [6,7]. These LCLs express similar gene sets that have been detected in EBV associated lymphoid malignancies in humans, such as immunoblasic B-cell lymphomas [1,2]. Transformation of B-lymphocytes by EBV has been attributed to the expression of a growth stimulatory program by the virus. LCLs express all EBV latency-associated genes, including six EBV nuclear antigens (EBNAs)—EBNA1, EBNA2, EBNA3A, EBNA3B, EBNA3C and EBNALP, three latent membrane proteins (LMPs)—LMP1, LMP2A, and LMP2B), two small noncoding RNAs (EBER1 and EBER2), and microRNA transcripts from the BHRF1 and BamHI A (BART) regions [1,2]. Out of these, five viral antigens including EBNA2, EBNA3A, EBNA3C, EBNA-LP and LMP1 act in concert to transform naïve B-

lymphocytes [8,9,10,11,12]. The EBNA3 family comprising of EBNA3A, EBNA3B, and EBNA3C genes are considered to comprise a family of non-redundant EBV genes, which most likely generated from gene duplication during primate gammaherpesvirus evolution [13,14,15]. Although the EBNA3 antigens possess the similar genomic structure, they share limited amino acid sequence homology within the N-terminal region [13,14,16].

The two major proteolytic cascades that cells use for protein degradation are the ubiquitin-proteasome system (UPS) and autophagy-lysosomal pathway [17,18]. In addition, another important family of cytosolic proteases is the caspases that cleave proteins after aspartic acid residues, also play an important role in protein degradation during apoptosis [19]. Although initially UPS and autophagy-lysosomal pathways were thought as self-governing protein degradation mechanisms, recent evidence suggests profound crosstalk between these two major protein turn-over mechanisms [18]. While the UPS typically degrades short-lived ubiquitinated proteins, autophagy-lysosomal pathway targets long-lived misfolded protein aggregates, which are produced in response to different cellular insults, such as growth factor deprivation, hypoxia and endoplasmic (ER) stress due to unfolded protein response (UPR) [20,21,22]. Autophagy is initiated by formation of a double membrane vesicle that encloses polyubiquitinated cargo protein aggregates through interacting with specific adaptor proteins, such as p62/SQSTM1. Subsequently, p62 interacts with microtubule-associated proteins 1A/1B light chain 3B (LC3B) via LC3-interacting region (LIR) motif [23,24]. LC3B is initially synthesized in an unprocessed form, pro-LC3, which is then cleaved at the C-terminal glycine residue into cytosolic form, LC3-I. Conjugation of phosphatidyl-ethanolamine (PE) to the C-terminal residue of LC3-I generates the membrane associated form, LC3-II, providing an authentic marker for autophagosome formation [25]. Subsequently, autophagosomes fuse with the lysosome to form autolysosome, where the acidic and hydrolytic environment helps to degrade the sequestered cargo protein aggregates [25,26].

The current study addressed the potential crosstalk among different degradation pathways with respect to EBNA3C degradation in EBV transformed B-lymphocytes. Previously it has been shown that EBNA3C can manipulate UPS either to stabilize cell oncoproteins (viz. Mdm2, Cyclin D1, c-Myc, Pim1) or enhance degradation of tumor suppressor proteins (viz. p53, $p27^{Kip1}$, pRb, $p21^{CIP1}$) [27,28,29,30,31,32]. In addition, EBNA3C is poly-ubiquitinated at the N-terminal region and interacts with the C8/α7 subunit of the 20S proteasome [28,33]. While *in vitro* EBNA3C along with two other family members are all degraded in the presence of 20S proteasome, in growing LCLs, EBNA3 proteins appear to be extremely stable, with no sign of UPS-mediated degradation [33]. Moreover, EBNA3C can bypass autophagy-lysosomal mediated degradation and subsequent antigen presentation for T-cell recognition [34,35]. Nevertheless, the underlying proteolytic mechanism that governs EBNA3C's turn-over remains yet to be determined. Recently, we have shown that EBNA3C transcriptionally activates autophagy machinery particularly when cells are under stressed conditions [36]. This autophagy activation appears to be essential for EBNA3C mediated latently infected B-cell survival. Moreover, EBNA3C expression in B-lymphocytes leads to accumulation of K63-linked poly-ubiquitinated protein aggregates directed for autophagy-lysosomal mediated degradation [36]. Herein we sought to investigate how EBNA3C protein degradation is regulated and the potential for targeting degradative pathways as a treatment strategy for various EBV associated B-cell lymphomas where EBNA3C is expressed.

Results

Proteasomal inhibition facilitates degradation of EBV essential nuclear antigen EBNA3C

Proteasomal inhibition leads to degradation of many important cell oncoproteins through autophagy-lysosomal pathway [37,38]. For example, expression of oncogenic mutant p53 is

significantly suppressed in cancer cells after treatment with proteasome inhibitors [37]. The prominent interaction of EBV essential antigen EBNA3C with the ubiquitin-proteasome system (UPS) [30,33] and autophagy-lysosomal pathway [36] led us to investigate the mechanism that governs the extraordinary stability of this viral oncoprotein in growing EBV transformed B-lymphocytes.

In order to determine the half-life of EBNA3C protein affected by UPS and autophagy-lysosomal pathway, EBV transformed lymphoblastoid cell line (LCL#1) was treated with protein synthesis inhibitor, cyclohexamide (CHX) for 24 h in the absence (DMSO control) or in the presence of proteasome (MG132, 1 μM) or autophagy-lysosomal (Chloroquine, CQ, 50 μM) inhibitors (Fig 1A). Beyond 24 h, the experiments became unreliable due to significant cell death induced by the treatment of different drugs. Samples were analyzed by western blotting (WB) of total protein extracts solubilized in lysis buffer and probing with antibodies directed against EBNA3C and GAPDH as loading control. Unexpectedly, the results demonstrated that instead of increasing EBNA3C stability, MG132 treatment resulted in a decrease of EBNA3C stability (half-life: ~12 h) in comparison to the DMSO treated cells (half-life: >24 h), whereas CQ treatment enhanced the overall EBNA3C protein stability (Fig 1A). To rule out the possible effect of MG132 in transcriptional regulation, a similar experimental set up was carried out using EBNA3C stably expressing BJAB cells (BJAB-E3C#7) (Fig 1B). As before, a parallel result was obtained (Fig 1B), indicating that MG132 mediated EBNA3C's degradation is likely controlled at the protein level.

Autophagy activation has been viewed as a compensatory protein degradation mechanism when proteasome function is inhibited [18,39]. In agreement to this, our results also demonstrated that MG132 treatment significantly increased LC3II conversion along with accumulation of poly-ubiquitinated proteins in HEK293 cells transiently transfected with either vector control or myc-tagged EBNA3C (Fig 1C). Autophagy activation upon MG132 treatment appears to be directly correlated with EBNA3C's degradation (Fig 1C). Upon normalization with GAPDH as loading control and GFP as transfection efficiency control, protein quantification revealed about 2 fold reduction in EBNA3C amount in MG132 treated cells as compared to DMSO treated cells, whereas CQ treatment caused no change or slight enhancement of EBNA3C amount as similar to the B-cells (Fig 1C). Earlier it has been demonstrated that MG132 treatment induces autophagy-lysosomal mediated degradation of mutant p53 in breast cancer cell lines [37]. Although p53 is wild-type in HEK293 cells [40], a similar degradation pattern was observed in our experiment (Fig 1C). However, Mdm2 expression was accumulated in MG132 treated cells (Fig 1C). Interestingly, no sign of EBNA3C's degradation was observed when autophagy was triggered in absence of growth promoting signals (Earle's Balanced Salt Solution, EBSS) for 9 h (Fig 1D). In contrast, a dose dependent degradative pattern of EBNA3C was observed with increasing concentrations of MG132 (0–40 μM) treated for 4 h (Fig 1E).

Previously, it has been shown that an internal glycine-alanine repeat domain of EBNA1 plays a critical role in inhibiting UPS mediated degradation as well as acts as a cis-inhibitor for MHC class I-restricted presentation through circumventing autophagy-lysosomal degradation mechanism [34,41,42]. In contrast to EBNA3C, no sign of degradation was observed for EBNA1 in response to MG132 treatment of transiently transfected HEK293 cells with (Fig 1F). Overall, the data suggest that proteasomal inhibition by MG132 enhances EBNA3C's degradation and autophagy-lysosomal pathway might play an important role in regulating EBNA3C stability.

Proteasomal inhibition leads to degradation of latent oncoproteins—EBNA3A and EBNA3C, but not EBNA3B

EBNA3 family members comprising EBNA3A, EBNA3B and EBNA3C share approximately 30% sequence homology near the N-terminal region [16]. All three EBNA3 proteins interact

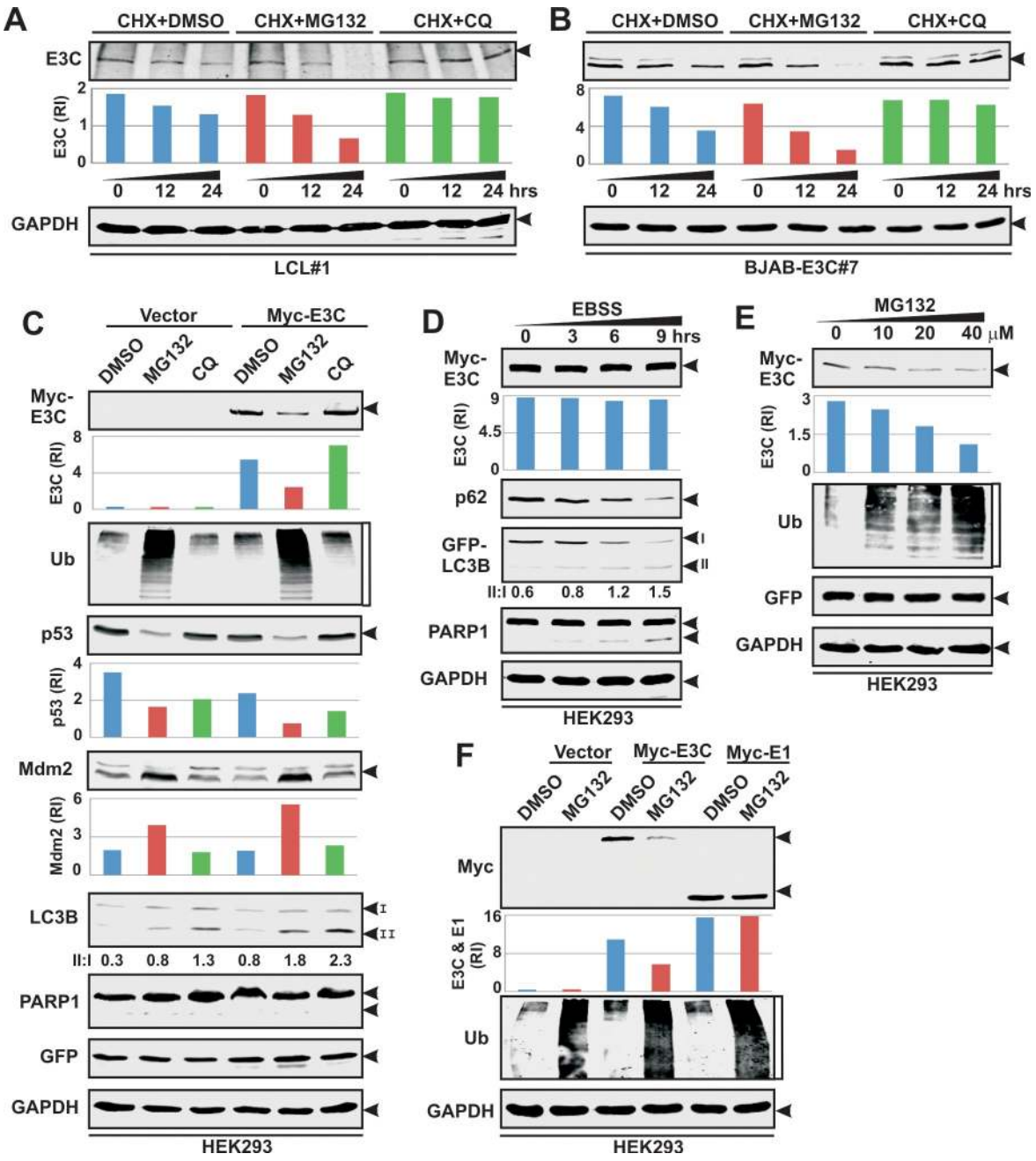

Fig 1. Proteasome inhibition leads to degradation of EBV essential antigen EBNA3C. (A) ~10 x 10^6 LCL#1 and (B) BJAB stably expressing EBNA3C (BJAB-E3C#7) cells were treated with protein synthesis inhibitor, cyclohexamide (CHX) for 24 h in the absence (DMSO control) or in the presence of 1 μM proteasome inhibitor MG132 or 50 μM autophagy-lysosomal inhibitor Chloroquine (CQ). (C) ~10 x 10^6 HEK293 cells transiently transfected with empty vector (pA3M) or pA3M-EBNA3C expressing myc-tagged EBNA3C. 36 h post-transfection cells were either left untreated (DMSO control) or treated with 20 μM MG132 or 50 μM CQ for another 4 h before harvesting. HEK293 cells transfected with myc-tagged EBNA3C were incubated with (D) EBSS to induce autophagy for 9 h or (E) increasing concentrations of MG132 (0–40 μM) for 4 h. (F) HEK293 cells transiently transfected with empty vector or expression plasmids for myc-tagged EBNA3C or EBNA1, were either left untreated or treated with 20 μM MG132 for additional 4 h. (A-F) In each experiment, cells were harvested after drug treatment, washed with 1 x PBS, lysed in RIPA and fractionated using appropriate SDS-PAGE. For transient transfection studies, cells were additionally transfected with GFP expression vector to monitor the transfection efficiency. Western blots were performed with indicated antibodies. GAPDH blot was performed as loading control. The relative intensities (RI) of protein bands shown as bar diagrams were quantified using the software provided by Odyssey CLx Imaging System. Representative gel pictures are shown of at least two independent experiments.

https://doi.org/10.1371/journal.ppat.1008105.g001

with C8 (α7) subunit of the 20S proteasome and are efficiently degraded *in vitro* in the presence of purified 20S proteasome [33]. However, *in vivo* in proliferating LCLs no sign of proteolytic degradation was observed for these proteins [33]. Moreover, EBNA3 proteins exert extensive cooperative functions and sometimes opposing activities [43,44]. While EBNA3A and EBNA3C are considered as viral oncoproteins by largely collaborating in growth promoting functions, EBNA3B exhibits tumor suppressive functions [8,9,45]. It was therefore important to determine whether EBNA3A and/or EBNA3B proteins were also similarly regulated in LCLs when proteasome was inhibited.

To this end, two LCLs–LCL#1 and LCL#89 were either left untreated (DMSO control) or treated with 1 μM MG132 and subjected to western blot analyses (Fig 2A). The results demonstrated that MG132 treatment resulted in a prominent decrease in expressions of both EBNA3A and EBNA3C viral oncoproteins, whereas unexpectedly no sign of degradation was observed for the third member of EBNA3 family proteins—EBNA3B, a non-essential viral latent antigen during B-cell transformation, in both LCLs (Fig 2A). A similar degradation pattern of both EBNA3A and EBNA3C was also found in BJAB cells stably expressing these viral oncoproteins (S1A and S1B Fig). Studies suggested that EBV encoded latent transmembrane oncoprotein LMP1 is a short-lived protein and unlike other cell plasma membrane substrates, it is degraded through both proteasomal and autophagy-lysosomal proteolytic mechanisms [46,47]. In agreement to this, our results also revealed that both proteasome inhibition by MG132 and blockade of lysosomal acidification by CQ considerably increased LMP1 expression as compared to the DMSO treated cells (Figs 2A and S1C). Interestingly, while MG132 treatment caused similar degradation pattern in both EBNA3A and EBNA3C, inhibition of autophagy-lysosomal pathway resulted in stabilization of only EBNA3C (S1C Fig). Effect of MG132 treatment was assessed by overall accumulation of polyubiquitinated proteins, induction of apoptosis as indicated by increased PARP1 cleavage and autophagy activation as shown by increased ratio of LC3II/I (Fig 2A). Interestingly, as similar to HEK293 experiments, MG132 treatment resulted in pronounced p53 degradation in both LCLs and BJAB cells stably expressing either EBNA3A or EBNA3C (Figs 2A and S1A–S1C). However, at this point we are not sure whether these LCLs (donor specific) express mutated or wild-type p53, since only mutated p53 was shown to be degraded in the presence of proteasomal inhibitors.

To corroborate proteasome inhibition mediated degradation of EBNA3 proteins, an immunofluorescence study was performed in LCL#89 without (DMSO) or with 1 μM MG132 treatment for 12 h (Fig 2B). As similar to the western blot analyses, the immunofluorescence results also demonstrated that MG132 treatment resulted in a decrease of staining intensities (~50%) for both EBNA3A and EBNA3C, but not EBNA3B (Fig 2B). To confirm or rule out the involvement of proteasome inhibition in EBNA3 protein degradation, another proteasome inhibitor bortezomib, a FDA approved drug against multiple myeloma [48], was also tested. Using a similar experimental set up, the results demonstrated that alike MG132, bortezomib also induced an effective degradation phenomenon of both EBNA3A and EBNA3C proteins (S1D Fig). Taken together, the results suggest that, impairment of proteasomal degradation machinery leads to specific degradation of EBV oncoproteins EBNA3A and EBNA3C and not the viral tumor suppressor protein EBNA3B through employing other proteolytic mechanism (s).

Proteasomal inhibition induces both viral and autophagy gene transcriptions

A number of potential therapeutic strategies have been described with transcriptional activation of EBV lytic genes using multiple chemotherapeutic agents such as HDAC inhibitor

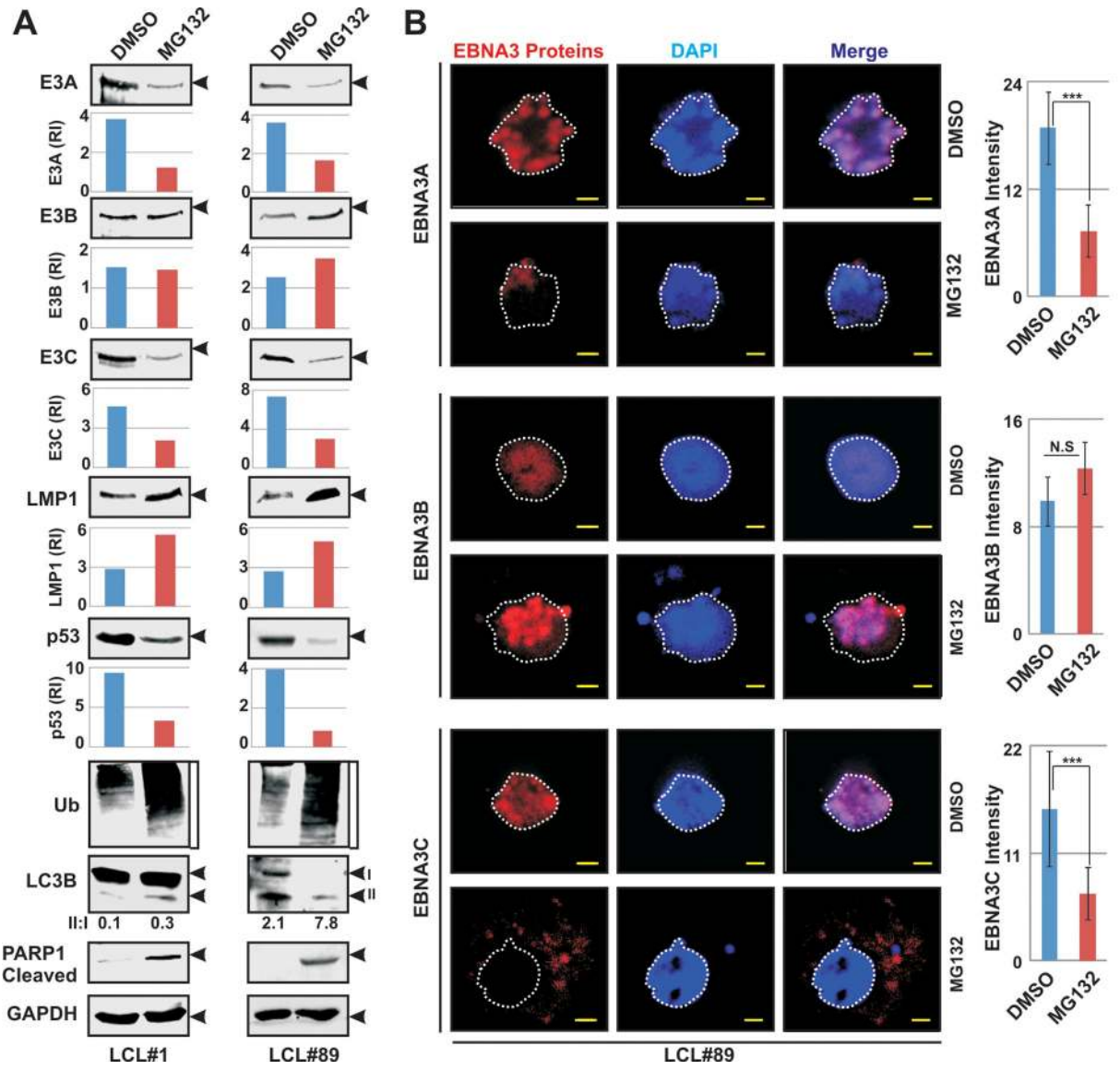

Fig 2. Proteasomal inhibition results in degradation of viral oncoproteins—EBNA3A and EBNA3C, but not EBNA3B in LCLs. (A) ~10 x 10^6 LCLs–both LCL#1 and LCL#89 were either left untreated (DMSO control) or treated with 1 μM MG132. 12 h post-incubation, cells were harvested, washed with 1 x PBS, lysed in RIPA buffer and subjected for western blot analyses with indicated antibodies. GAPDH blot was used as loading control. The relative intensities (RI) of protein bands shown as bar diagrams were quantitated using the software provided by Odyssey CLx Imaging System. Representative gel pictures are shown of at least two independent experiments. (B) For confocal assays, ~5 x 10^4 LCLs (LCL#89) either left untreated (DMSO control) or treated with 1 μM MG132 for 12 h, were fixed with 4% paraformaldehyde. Immunostaining was performed using primary antibodies against viral proteins—EBNA3A, EBNA3B and EBNA3C followed by Alexa Fluor conjugated secondary antibodies for visualization in a Leica DMi8 Confocal Laser Scanning Microscope. All panels are representative pictures of two independent experiments. The bar diagram represents the mean value of staining intensities of EBNA3 proteins from at least 10 cells of 3 different fields. *** indicates $P < 0.05$. Nuclei were counterstained using DAPI (4',6'-diamidino-2-phenylindole) before mounting the cells.

https://doi.org/10.1371/journal.ppat.1008105.g002

(sodium butyrate; NaBu) in combination with a protein kinase C activator (12-O-tetradecanoylphorbol-13-acetate; TPA) [49,50,51]. Additionally, proteasome inhibitor, bortezomib treatment can also enhance EBV lytic gene transcription where CCAAT/enhancer-binding protein β (C/EBPβ) plays an important role in transactivating BZLF1 through binding to its promoter region [52]. However, the effect of proteasomal inhibition on other viral genes–both lytic and latent was not explored. To evaluate the effect of proteasomal inhibition at the

transcriptional level of viral genes, quantitative reverse transcription–polymerase chain reaction (qRT–PCR) assays were performed in LCLs either left untreated (DMSO control) or treated with proteasome inhibitors—MG132 (Fig 3A and 3C) and bortezomib (S2A and S2C Fig). The results demonstrated that proteasomal inhibition robustly enhanced both lytic and latent genes transcription including EBNA3A and EBNA3C, in contrast to its effect at their protein levels (Figs 3A, 3C, S2A and S2C). In order to rule out any aberrant transcriptional regulation due to proteasome inhibition, we have utilized three housekeeping genes–*B2M*, *RPLPO* and *GAPDH* demonstrating minimal change in the absence and presence of drugs. Transcriptional activation of lytic genes led us to further investigate whether proteasomal inhibition could also induce EBV lytic cycle activation. In agreement to the previously demonstrated experiment with bortezomib [52], our results also showed a similar trend of EBV lytic cycle activation in both proteasome inhibitors (MG132 and bortezomib) and NaBu/TPA treated LCLs compared to control cells (Figs 3B, 3D, S2B and S2D).

To further investigate the global effect of proteasomal inhibition at transcriptional level, RNA-seq experiment was conducted and analyzed the transcript levels of genes that are deregulated in LCLs upon MG132 treatment (Fig 3E and 3F and S1 Table). The results demonstrated that upon MG132 treatment there was a significant increase in the transcripts levels of genes involved in either autophagy activation (p62/*SQSTM1*, *MAP1LC3B*, *GABARAPL1*, *CTSD*, *UBC*), or protein folding and regulation of cellular response to various cellular insults such as unfolded protein response (UPR) and chaperone mediated autophagy (*HSPH1*, *HSP90AA1*, *HSPA2*, *HSPB1*, *DNAJB1*, *DNAJB4*, *SERPINH1*, *HSPA8*, *HSP90AA4P*, *HSP90AB3P*, *BAG3*) as compared to the control LCLs (Fig 3E and 3F). On the other hand, proteasomal inhibition caused a drastic reduction of mRNA levels of genes particularly involved in DNA replication and nucleosome assembly (Fig 3E and 3F). The RNA-seq data for autophagy (p62/*SQSTM1*, *MAP1LC3B*, *GABARAPL1*, and *CTSD*) and chaperone (*HSP90AA1* and *HSPA8*) gene transcriptions were further validated by qRT-PCR assays in LCLs in the absence and presence of proteasome inhibitors (Figs 3G, 3H, S2E and S2F).

To further assess transcriptional regulation of EBNA3 genes, qRT-PCR analyses were performed in BJAB cells stably expressing either EBNA3A (BJAB#E3A) or EBNA3C (BJAB#E3C) under viral CMV promoter with or without MG132 treatment (S2G and S2H Fig, respectively). The results demonstrated unlike enodogenous promoter in LCLs, proteasome inhibition did not alter EBNA3A or EBNA3C transcripts in the hetorologous expression system (S2G and S2H Fig). However, as similar to LCLs, proteasome inhibition caused transcriptional activation of the selected autophagy and chaperone genes in both EBNA3A and EBNA3C expressing BJAB cells (S2G and S2H Fig). Notably, upon proteasomal inhibition, as compared to EBNA3A expressing cells, a significant higher ($>\log_{10}$ 10 fold) transcriptional activation of these genes were observed in EBNA3C expressing cells (Compare S2G and S2H Fig).

Previously it has been demonstrated that intronic sequences can influence expressions of EBNA3 family proteins and intron retention provides a mechanism for the fine tuning of expression of the individual EBNA3 family genes [53]. In order to determine whether proteasomal inhibition could influence splicing of EBNA3 genes, two different sets of primers were designed for qRT-PCR analyses (S3A Fig and S2 Table). While the first primers set detected the presence of intronic sequence, second set of primers determined only exonic region (S3A Fig). The efficiency of both primer sets were determined by qRT-PCR analyses (S3B Fig). The results demonstrated that proteasome inhibition caused transcriptional activation of all three EBNA3 genes at similar level as detected by both sets of primers (S3B Fig). In agreement to the previous study, agarose gel electrophoresis of PCR end products also confirmed that in EBV transformed LCLs (both LCL#1 and LCL#89) EBNA3 genes retained their intronic sequences and in addition proteasomal inhibition did not affect splicing of EBNA3 genes (S3C Fig).

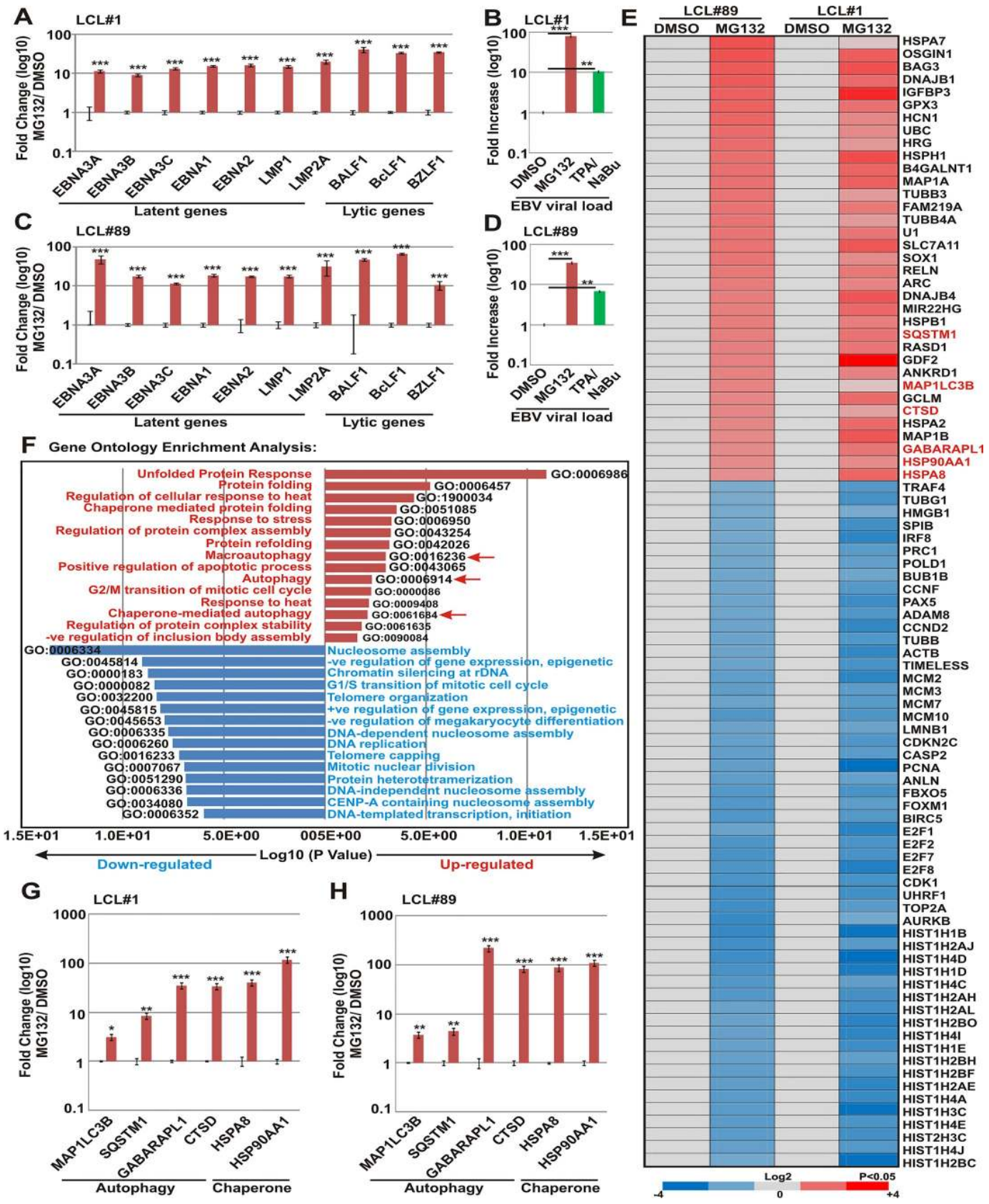
A
LCL#1
Fold Change (log10) MG132/ DMSO
EBNA3A
EBNA3B
EBNA3C
EBNA1
EBNA2
LMP1
LMP2A
BALF1
BcLF1
BZLF1
Latent genes
Lytic genes
B
LCL#1
Fold Increase (log10)
DMSO
MG132
TPA/ NaBu
EBV viral load
C
LCL#89
D
LCL#89
E
LCL#89
LCL#1
DMSO
MG132
HSPA7
OSGIN1
BAG3
DNAJB1
IGFBP3
GPX3
HCN1
UBC
HRG
HSPH1
B4GALNT1
MAP1A
TUBB3
FAM219A
TUBB4A
U1
SLC7A11
SOX1
RELN
ARC
DNAJB4
MIR22HG
HSPB1
SQSTM1
RASD1
GDF2
ANKRD1
MAP1LC3B
GCLM
CTSD
HSPA2
MAP1B
GABARAPL1
HSP90AA1
HSPA8
TRAF4
TUBG1
HMGB1
SPIB
IRF8
PRC1
POLD1
BUB1B
CCNF
PAX5
ADAM8
CCND2
TUBB
ACTB
TIMELESS
MCM2
MCM3
MCM7
MCM10
LMNB1
CDKN2C
CASP2
PCNA
ANLN
FBXO5
FOXM1
BIRC5
E2F1
E2F2
E2F7
E2F8
CDK1
UHRF1
TOP2A
AURKB
HIST1H1B
HIST1H2AJ
HIST1H4D
HIST1H1D
HIST1H4C
HIST1H2AH
HIST1H2AL
HIST1H2BO
HIST1H4I
HIST1H1E
HIST1H2BH
HIST1H2BF
HIST1H2AE
HIST1H4A
HIST1H3C
HIST1H4E
HIST2H3C
HIST1H4J
HIST1H2BC
Log2
P<0.05
-4
0
+4
F
Gene Ontology Enrichment Analysis:
Unfolded Protein Response
Protein folding
Regulation of cellular response to heat
Chaperone mediated protein folding
Response to stress
Regulation of protein complex assembly
Protein refolding
Macroautophagy
Positive regulation of apoptotic process
Autophagy
G2/M transition of mitotic cell cycle
Response to heat
Chaperone-mediated autophagy
Regulation of protein complex stability
-ve regulation of inclusion body assembly
GO:0006986
GO:0006457
GO:1900034
GO:0051085
GO:0006950
GO:0043254
GO:0042026
GO:0016236
GO:0043065
GO:0006914
GO:0000086
GO:0009408
GO:0061684
GO:0061635
GO:0090084
GO:0006334 Nucleosome assembly
GO:0045814 -ve regulation of gene expression, epigenetic
GO:0000183 Chromatin silencing at rDNA
GO:0000082 G1/S transition of mitotic cell cycle
GO:0032200 Telomere organization
GO:0045815 +ve regulation of gene expression, epigenetic
GO:0045653 -ve regulation of megakaryocyte differentiation
GO:0006335 DNA-dependent nucleosome assembly
GO:0006260 DNA replication
GO:0016233 Telomere capping
GO:0007067 Mitotic nuclear division
GO:0051290 Protein heterotetramerization
GO:0006336 DNA-independent nucleosome assembly
GO:0034080 CENP-A containing nucleosome assembly
GO:0006352 DNA-templated transcription, initiation
1.5E+01
1.0E+01
5.0E+00
005E+00
5.0E+00
1.0E+01
1.5E+01
Down-regulated
Log10 (P Value)
Up-regulated
G
LCL#1
Fold Change (log10) MG132/ DMSO
MAP1LC3B
SQSTM1
GABARAPL1
CTSD
HSPA8
HSP90AA1
Autophagy
Chaperone
H
LCL#89

Fig 3. Proteasomal inhibition induces both viral and autophagy gene transcriptions. (A-D) ~10 x 10^6 two LCL clones–LCL#1 and LCL#89 were either left untreated (DMSO control) or treated with 1 μM MG132. 12 h post-treatment cells were harvested for (A and C) total RNA or (B and D) genomic DNA isolation as described in the "Materials and Methods" section. (B and D) LCLs were treated with 3 mM sodium butyrate (NaBu) in combination with 20 ng/ml 12-O-tetradecanoylphorbol-13-acetate (TPA) for 24 h to induce viral lytic cycle as positive control. (A and C) Total RNA was subjected to cDNA preparation followed by quantitative real-time PCR (qPCR) analyses for the selected viral genes. The relative changes in transcripts (log10) using the $2^{-\Delta\Delta Ct}$ method are represented as bar diagrams in comparison to DMSO control using GAPDH, B2M and RPLPO as housekeeping genes. Two independent experiments were carried out in similar settings and results represent as an average value for each transcript. (B and D) qPCR was performed for the detection of EBV DNA (BamHW fragment) using the genomic DNA isolated from each sample. The average fold increase of two independent experiments represented as bar diagrams was calculated in comparison to DMSO control using the $2^{-\Delta\Delta Ct}$ method taking GAPDH as genomic control. (A-D and G-H) Average values +/- SEM are plotted. *, **, *** = p-value < 0.01, 0.005 and 0.001 respectively. (E) The cDNA samples similarly prepared in (B and D) were subjected to whole transcriptome analyses (RNA-Seq) using Ion S5 XL System as described in the "Materials and Methods" section. RNASeqAnalysis plugin (v5.2.0.5) was utilized to perform the analysis after align with human genome (hg19) and produce gene counts for all the samples. Differential gene expressions were performed based on p-value as $< = 0.05$ and $\log_2$ Fold Change as 2 and above (upregulated, red) and -2 and below (downregulated, blue). (F) Differentially expressed gene sets were uploaded on DAVID v6.8 webserver for functional analysis. Gene Ontology (GO) was selected from the hits table for DAVID clustering. The bar diagrams (upregulated: red; downregulated: blue) represent top 15 most significantly affected pathways. (G-H) qPCR analyses of the selected cellular genes as described in (A and C).

https://doi.org/10.1371/journal.ppat.1008105.g003

Autophagy stimulated by proteasomal inhibition is required for the degradation of EBNA3C

Autophagy activation as confirmed by both western blot and RNA-Seq analyses upon MG132 treatment, prompted us to further investigate that whether autophagy-lysosomal pathway is responsible for EBNA3C degradation when proteasome is inhibited. To this end autophagy pathway was either blocked by chemical inhibitors—bafilomycin (0.1 μM) or chloroquine (CQ; 50 μM) treatment or by Beclin 1 knockdown (Fig 4). While bafilomycin blocks the fusion between autophagosome and lysosome, CQ increases the lysosomal pH and thereby blocks protein degradation. Beclin 1 is one of the initial components that initiate autophagosome formation. First, LCLs either left untreated (DMSO control) or treated with MG132 in the absence and presence of bafilomycin were subjected to both western blot and confocal analyses (Fig 4A and 4B, respectively). The results demonstrated that MG132 induced EBNA3C degradation was partially inhibited by bafilomycin treatment (Fig 4A). While confocal analyses further corroborated this notion, MG132 along with bafilomycin treatment caused a significant accumulation of EBNA3C protein in the cytoplasmic fraction colocalized with LC3B, indicating that proteasomal inhibition led to cytoplasmic translocation of EBNA3C for degradation (Fig 4B).

A similar degradation pattern of EBNA3C in response to proteasomal inhibition and possible involvement of autophagy pathway was further validated in transient expression system (Fig 4C and 4D). EBNA3C degradation induced by proteasomal inhibition was substantially restored by both CQ treatment and beclin 1 knockdown condition (Fig 4C and 4D, respectively). HEK293 cells were stably knockdown for Beclin1 by transfecting a lentiviral sh-Beclin1 expressing construct under doxycycline inducible promoter (Fig 4D). Unlike EBNA3C, MG132 induced p53 (endogenous) degradation was fully restored when cells were co-treated with CQ (Fig 4C). Both LC3B and p62 were used to evaluate the autophagy level and as expected, LC3B-II/I ratios were increased following MG132 treatment alone and with autophagy inhibitors, concomitantly with the EBNA3C expression levels (Fig 4A and 4C). Accumulation of poly-ubiquitinated proteins were also detected in accordance with MG132 treatment (Fig 4A, 4C and 4D).

To further validate EBNA3C degradation induced upon MG132 treatment and its possible dynamics with autophagy machinery, live cell confocal microscopy analysis was conducted in doxycycline inducible sh-Beclin 1 stably expressing HEK293 cells transiently transfected with GFP-EBNA3C expressing construct (Fig 4E). The results demonstrated a drastic reduction of overall EBNA3C puncta upon MG132 treatment as compared to DMSO control in the absence of doxycycline (active autophagy machinery) (Fig 4E, upper panels). On the contrary, in the

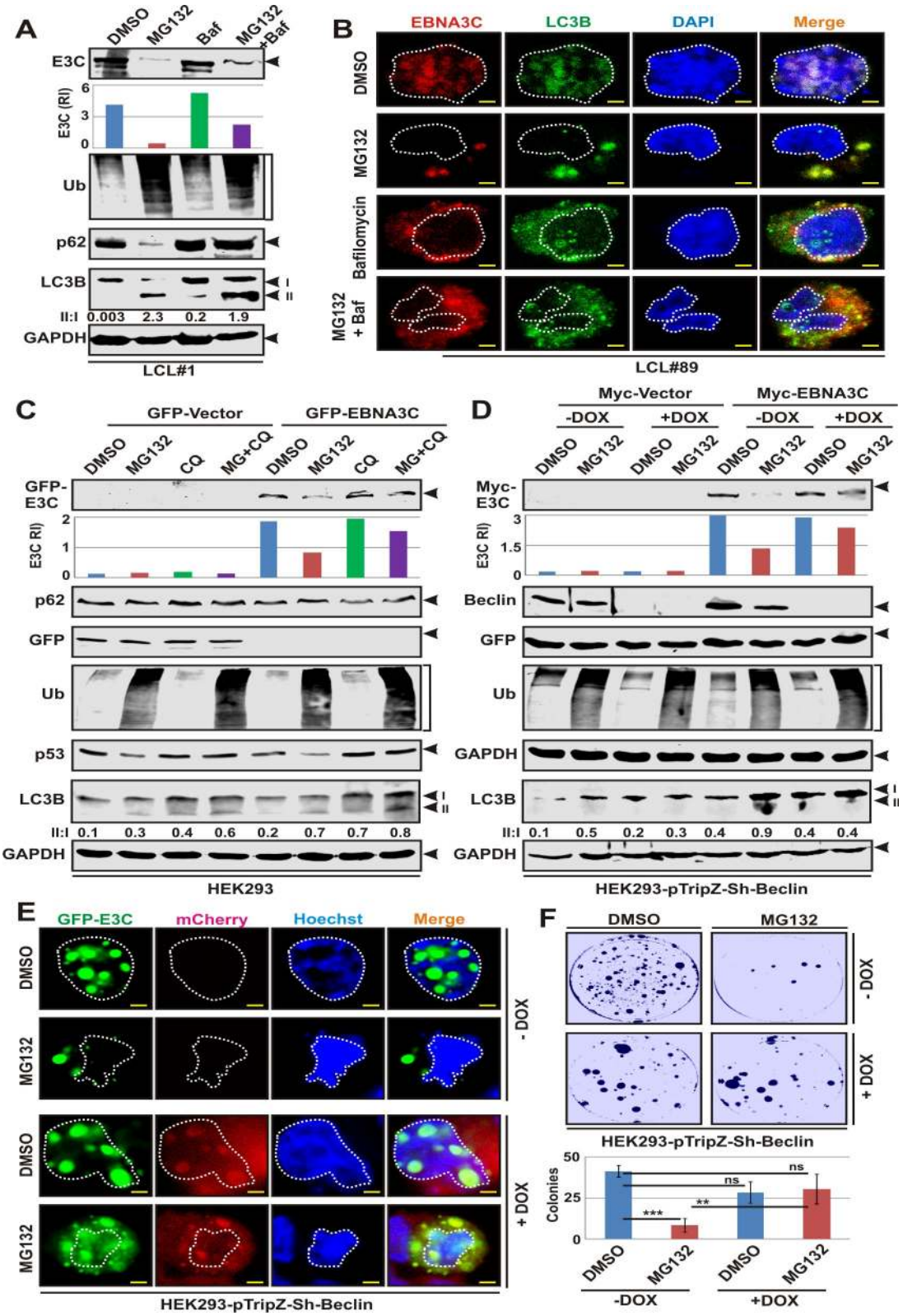

Fig 4. EBNA3C is degraded through autophagy-lysosomal pathway when proteasome is inhibited. LCLs were either left untreated (DMSO control) or treated with 1 μM MG132, 0.1 μM bafilomycin (Baf) or MG132 plus Baf. 24 h post-treatment cells were subjected for either (A) western blot analysis or (B) immunostaining with the indicated antibodies. Each panel in (B) is

representative picture of two independent experiments and nuclei were counterstained by DAPI before mounting the cells. Scale bars, 5 μm. (C) ~10 x 10^6 HEK293 cells transfected with either empty vector (pEGFP-C1) or GFP-tagged EBNA3C expression plasmid, either left untreated (DMSO control), or treated with 20 μM MG132 alone or MG132 plus 50 μM chloroquine (CQ). (D) HEK293 cells stably transfected with pTripz-mCherry-Sh-Beclin1 construct expressing sh-Beclin 1 under doxycycline (Dox) inducible promoter were further transfected either empty vector (pA3M) or myc-tagged EBNA3C expressing construct. 36 h post-transfection cells were either left untreated or treated with 20 μM MG132. (C-D) 4 h post-treatment cells were harvested, washed with 1 x PBS, lysed in RIPA buffer and subjected for western blot analyses for the indicated antibodies. (E) ~5 x 10^4 HEK293 cells stably expressing sh-Beclin 1 with or without doxycycline treatment were transfected with GFP-tagged EBNA3C expressing plasmid using Lipofectamine 3000. 24 h post transfection cells were either left untreated (DMSO control) or treated with 20 μM MG132 for another 4h and subjected to live cell confocal analysis after staining the nucleus with Hochest 33342. Doxycycline treatment induces both mCherry and sh-RNA expression. Scale bars, 5 μm. (F) A colony formation assay was conducted as described in the "Materials and Methods" section using a similar experimental setup in doxycycline inducible sh-Beclin1 stably expressing HEK293 cells transiently transfected with GFP-EBNA3C construct.

https://doi.org/10.1371/journal.ppat.1008105.g004

presence of doxycycline (Beclin 1 knockdown) MG132 treatment could not induce EBNA3C degradation as indicated by accumulation of GFP-EBNA3C puncta throughout the cell, predominantly in the cytoplasmic compartment (Fig 4E, lower panels).

In order to assess whether or not proteasomal inhibition promotes EBNA3C degradation and thereby affecting its oncogenic potential, a colony formation assay was conducted using a similar experimental setup in doxycycline inducible sh-Beclin 1 stably expressing HEK293 cells transiently transfected with GFP-EBNA3C construct as described above (Fig 4F). Indeed, the results demonstrated that impairment of autophagy pathway (Beclin 1 knockdown) partially reinstated EBNA3C colony formation ability when proteasome is blocked (Fig 4F). Overall the results suggest that the increased degradation of EBNA3C complementing with reduced oncogenic potential observed with MG132 treatment was mediated at least in part by the autophagy-lysosomal pathway.

EBNA3C interacts and colocalizes with p62-LC3B complex in the cytoplasmic fraction when proteasome is compromised

It has been demonstrated that p62/SQSTM1 directly binds to LC3B to facilitate degradation of ubiquitinated protein substrates by autophagy-lysosomal pathway [23]. To determine whether EBNA3C can participate within the p62-LC3B complex, HEK293 cells transiently transfected with either empty vector or flag-EBNA3C expressing construct, were subjected to immunoprecipitate with anti-flag monoclonal antibody (M2) with or without exposure of 20 μM MG132 for 4 h (Fig 5A). The results demonstrated that EBNA3C forms a stable complex with both p62 and LC3B, irrespective of proteasomal activities (Fig 5A). In order to validate the interaction of EBNA3C with p62-LC3B complex in a more endogenous setting, a similar immunoprecipitation experiment was carried out in LCLs (Fig 5B). p62-LC3B complex was evidently precipitated with EBNA3C pull-down using a mouse monoclonal antibody (A10) in DMSO treated LCLs (Fig 5B). However, owing to severe degradation of EBNA3C as well as p62 (increase of autophagy flux) in MG132 (1 μM, 12 h) treated LCLs resulted in lack of effective protein concentrations and accordingly no complex formation was detected when pull-down with anti-EBNA3C antibody as similar to mouse IgG control (Fig 5B).

To corroborate the association of EBNA3C with p62-LC3B complex and degradation pattern in the absence or presence of MG132, colocalization experiments were carried out using both ectopic (HEK293) and endogenous (LCLs) expressing systems (Fig 5C and 5D, respectively). First, HEK293 cells grown on glass bottom dishes were transiently transfected with RFP-tagged EBNA3C and GFP-tagged LC3B or GFP-tagged EBNA3C and mCherry-tagged p62 (Fig 5C). Cells were further treated with 10 μM MG132 for 4h or left untreated (DMSO control) and subjected for live cell confocal microscopy analyses (Fig 5C). The results

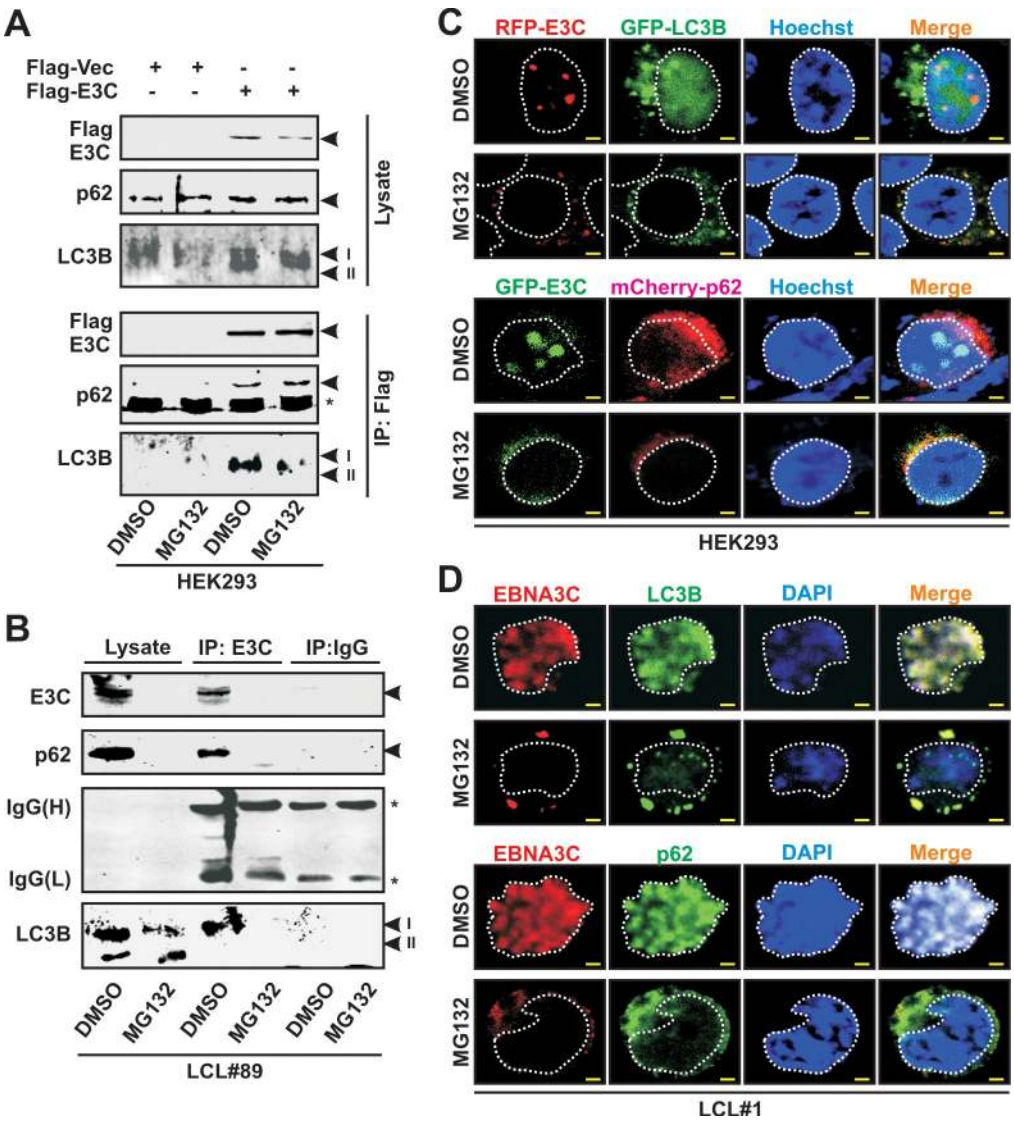

Fig 5. EBNA3C participates within the p62-LC3B complex when proteasome is inhibited. (A) ~10 x 10^6 HEK293 cells were transfected with either empty vector (pA3F) or flag-tagged EBNA3C expressing construct. 36h post-transfection cells were either left untreated (DMSO control) or treated with 20 μM MG132 for 4 h. After treatment, cells were harvested and subjected for immunoprecipitation with anti-flag antibody (M2). Precipitated products along with 10% whole cell lysates were run on gel and western blot analysis was performed with indicated antibodies. (B) ~20 x 10^6 LCLs (LCL#89) either left untreated (DMSO control) or treated with 1 μM MG132 for 12 h, were harvested and subjected for immunoprecipitation using EBNA3C specific mouse monoclonal antibody (A10). Rabbit anti-mouse IgG was used as isotype control. (C) ~5 x 10^4 HEK293 cells were co-transfected with the indicated expression plasmids using Lipofectamine 3000. 36 h post transfection, cells were further treated with DMSO or 20 μM MG132 for 4 h and subjected for live cell confocal analysis after staining the nucleus with Hochest 33342. (D) For confocal analysis in LCLs, ~5 x 10^4 LCLs (LCL#1) were treated with DMSO control or 1 μM MG132 for 12 h and subjected for immune staining with EBNA3C, p62, LC3B specific primary antibodies followed by incubation with Alexa Fluor conjugated secondary antibodies. Nuclei were counterstained using DAPI (4',6'-diamidino-2-phenylindole) before mounting the cells. Each panel in (C-D) corresponds to single experiment of three independent experiments. Scale bars, 5 μm.

https://doi.org/10.1371/journal.ppat.1008105.g005

demonstrated that MG132 treatment caused a drastic reduction of EBNA3C puncta formation in the nucleus compartments and increase in colocalization with both LC3B and p62 independently in the cytoplasmic fraction (Fig 5C). A similar colocalization pattern of EBNA3C with LC3B and p62 was also observed in LCLs upon MG132 treatment (Fig 5D).

Participation of EBNA3C within p62-LC3B complex prompted us to further investigate whether p62 acts as an adaptor for EBNA3C degradation through autophagy-lysosomal pathway. To this end, HEK293 cells were stably knockdown for p62 by transfecting a lentiviral sh-p62 expressing construct under doxycycline inducible promoter (S4A Fig). The efficiency of p62 knockdown was confirmed by both qRT-PCR and western blot analyses (S4B and S4C Fig, respectively). Next, this HEK293 cells stably expressing sh-RNA against p62 with or without doxycycline treatment for 48 h were transiently transfected with myc-EBNA3C expressing construct. 24 h post-transfection cells were either left untreated (DMSO control) or treated with MG132 and subjected to western blot analyses (S4D Fig). The results demonstrated that EBNA3C degradation induced by MG132 treatment was partially rescued when p62 expression was depleted in the presence of doxycycline treatment (S4D Fig). Overall, the results indicated that p62-LC3B binds to EBNA3C in physiological conditions, mediating its degradation via the autophagy-lysosomal pathway when proteasome is inhibited.

EBNA3C is predominantly K63-linked polyubiquitinated when proteasome is inhibited

Studies suggested that proteins modified with K48-linked ubiquitin chains are targeted for the proteasomal pathway, whereas K63-linked chains can target substrates for degradation via autophagy [54,55]. Previously it has been shown that EBNA3C can be polyubiquitinated at the N-terminal domain [28]. However, whether this polyubiquitination is K48-linked or K63-linked is still unclear. In addition, the UBA (ubiquitin associated) domain of p62 can bind to both K48- and K63-linked (with a higher affinity) polyubiquitin chains and regulate autophagic protein turnover [56]. These led us to further investigate the nature of polyubiquitinated chains associated with EBNA3C in the absence or presence of MG132. Immunofluorescence assays using specific antibodies against EBNA3C, total ubiquitin, K48- and K63-linked polyubiquitin chains in LCLs either left untreated (DMSO control) or treated with MG132, demonstrated that EBNA3C largely colocalized with ubiquitin irrespective of its type of chains within the nuclear compartments under physiological conditions (DMSO control), while MG132 treatment resulted in alteration of colocalization pattern from nuclear to predominantly cyctoplasmic along with drastic reduction of overall EBNA3C staining intensities (Fig 6A). Using a similar experimental set up, western blot analyses of LCLs confirmed that MG132 treatment significantly enhanced both total ubiquitination and K48-linked polyubiquitination levels designated for proteasomal mediated degradation (Fig 6B). In contrast, together with EBNA3C, K63-linked polyubiquitination level was notably decreased in MG132 treated LCLs, indicating that K63-linked polyubiquitinated substrates (including EBNA3C) are recycled in autophagy-lysosomal pathway, when proteasome is inhibited (Fig 6B). Full blot analyses of EBNA3C (~120 kDa) western blots using two different antibodies (mouse monoclonal followed by a sheep polyclonal) demonstrated the degradation/proteolytic cleavage pattern, identifying two predominant bands–one at ~75 kDa and another at ~45 kDa (Fig 6B).

To precisely determine EBNA3C specific poyubiquitnation pattern as well as to rule out the possible involvement of other viral oncoproteins, ectopic expression system was utilized where HEK293 cells were transiently transfected with either vector control or myc-tagged EBNA3C (Fig 6C). The results demonstrated that presence of EBNA3C enhanced overall ubiquitination levels along with K48- and K63-linked polyubiqutinated chains in physiological conditions (DMSO control) as compared to empty vector (Fig 6C). MG132 treatment further enhanced both total and K48-linked polyubiquitination, while significantly declined K63-linked polyubiquitination level in EBNA3C expressing cells (Fig 6C), corroborating the previous experiments in LCLs. To validate EBNA3C polyubiquitination pattern, *in vivo* ubiquitination experiments

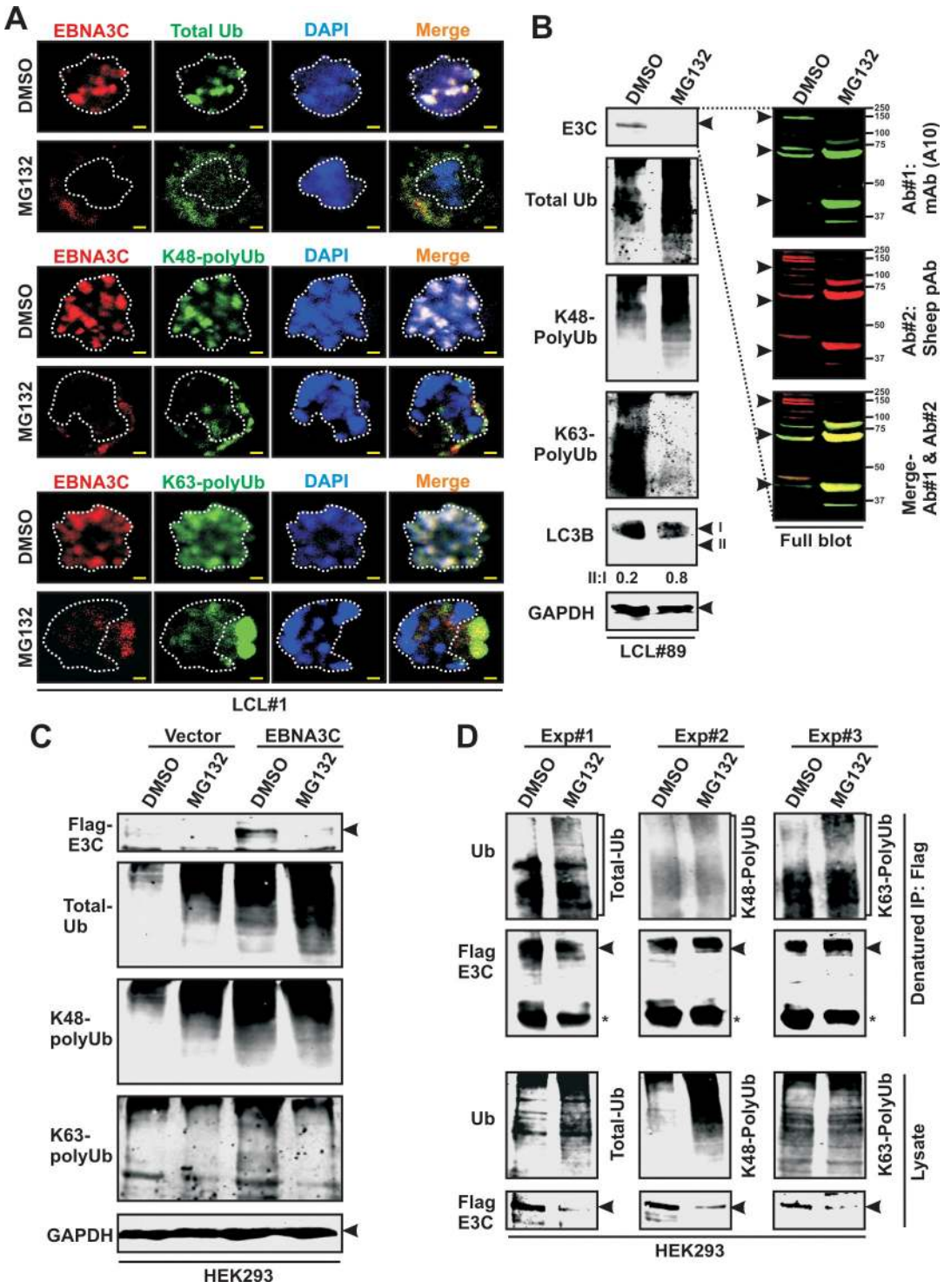

Fig 6. EBNA3C is predominantly K63-linked polyubiquitinated when proteasome is inhibited. LCLs were either left untreated (DMSO control) or treated with 1 μM MG132 for 12 h and subjected for (A) immunostaining with EBNA3C, total ubiquitin (Ub), K48- and K63-linked polyubiqitination specific antibodies; (B) western blot analyses with indicated antibodies. (A) Nuclei were counterstained with DAPI before mounting the cells for confocal analyses. (C-D) HEK293 cells transiently transfected with flag-tagged EBNA3C expression vector, either left untreated (DMSO control) or treated with 20 μM MG132 for 4h were subjected for (C) western blot analyses or (D) immunoprecipitation (IP) under denatured conditions using anti-flag antibody followed by western blot analyses using indicated antibodies. Each panel in (A) corresponds to single experiment of two independent experiments. Scale bars, 5 μm. Western blots in (B-C) were performed by stripping and reprobing the membranes with different antibodies.

https://doi.org/10.1371/journal.ppat.1008105.g006

was conducted in the absence and presence of MG132 in denaturing conditions allowing only covalent modifications (Fig 6D). The results demonstrated that MG132 treatment specifically enhanced K63- but not K48-linked polyubiquitination of EBNA3C (Fig 6D).

N-terminal domain of EBNA3C is important for autophagy mediated degradation in response to proteasomal inhibition

Earlier demonstration of polyubiquitination at the N-terminal domain (residues 1–159) of EBNA3C [28] led us to further explore the domain(s) responsible for autophagy mediated degradation in response to proteasomal inhibition. To this end, HEK293 cells were transiently transfected with flag-tagged EBNA3C constructs expressing EBNA3C residues 1–365 (N-terminal), residues 366–620 (middle part) and residues 621–992 (C-terminal). As described earlier, 36h post-transfected cells were either left untreated (DMSO control) or treated with MG132 (20 μM) or CQ (50 μM) for another 4 h (Figs 7A and S5A for high exposure). The results demonstrated that only MG132 treatment caused significant reduction in expression of EBNA3C N-terminal domain as compared to DMSO or CQ treated cells (Figs 7A and S5A). However, there was little or no change of ectopic expression levels of other two domains ranging from residue 366 to residue 992 in the absence or presence of both proteasomal and autophagy inhibitors (Figs 7A and S5A). LC3II conversion confirmed autophagy activation, while enhanced polyubiquitination validated effective proteasomal inhibition upon MG132 treatment (Fig 7A). *In vivo* ubiquitination experiments also validated polyubiquitination of EBNA3C at the N-terminal domain (residues 1–365) both in physiological conditions (DMSO control) and when proteasome is inhibited by MG132 (Fig 7B).

To identify whether the N-terminal domain contains any proteolytic cleavage site, full length EBNA3C sequence was searched for the presence of putative PEST (proline, glutamic acid, serine and threonine) sequences. Near the N-terminal domain (residues 28–44) a potential PEST sequence 'HDQDPGPGPPSSGASER' was identified (Fig 7C). In order to determine whether this identified PEST sequence is responsible for autophagy dependent degradation in response to proteasomal inhibition, three more flag-tagged EBNA3C truncated constructs were generated expressing residues 50–300 (lacking PEST motif), residues 1–300 and residues 1–250. HEK293 cells transiently transfected with these constructs along with EBNA3C residues 1–365 expressing plasmid were subjected to western blot analyses after treatment with either DMSO control or MG132 (Figs 7D and S5B for high exposure). While MG132 treatment caused obvious stabilization of residues 50–300, significant reduction of protein expression was observed when first 50 residues were included in all three EBNA3C truncations (Figs 7D and S5B). Taken together, the results indicated that EBNA3C N-terminal first 50 residues containing PEST sequence might be responsible for autophagy-lysososmal mediated degradation when proteasome is inhibited.

EBNA3C N-terminal domain is degraded in the both nuclear and cytoplsamic fractions upon proteasomal inhibition

In order to continue exploring the mechanisms involved in EBNA3C degradation, full length EBNA3C sequence was investigated for potential leucine-rich nuclear export signal (NES) motifs in NetNES 1.1 Server [57]. Two predicted NES sequences of EBNA3C were determined near the N-terminal (residues 124–132 "LQALSNLIL") and C-terminal (residues 862–869 "LQLSLVPL") regions (Fig 8A). However, interestingly, no predicted NES sequences were found for both EBNA3A and EBNA3B proteins. To confirm this prediction, a subcellular fractionation was performed using HEK293 cells transiently transfected with myc-EBNA3C (Fig 8B). The results demonstrated that EBNA3C was indeed fractionated in both nuclear and

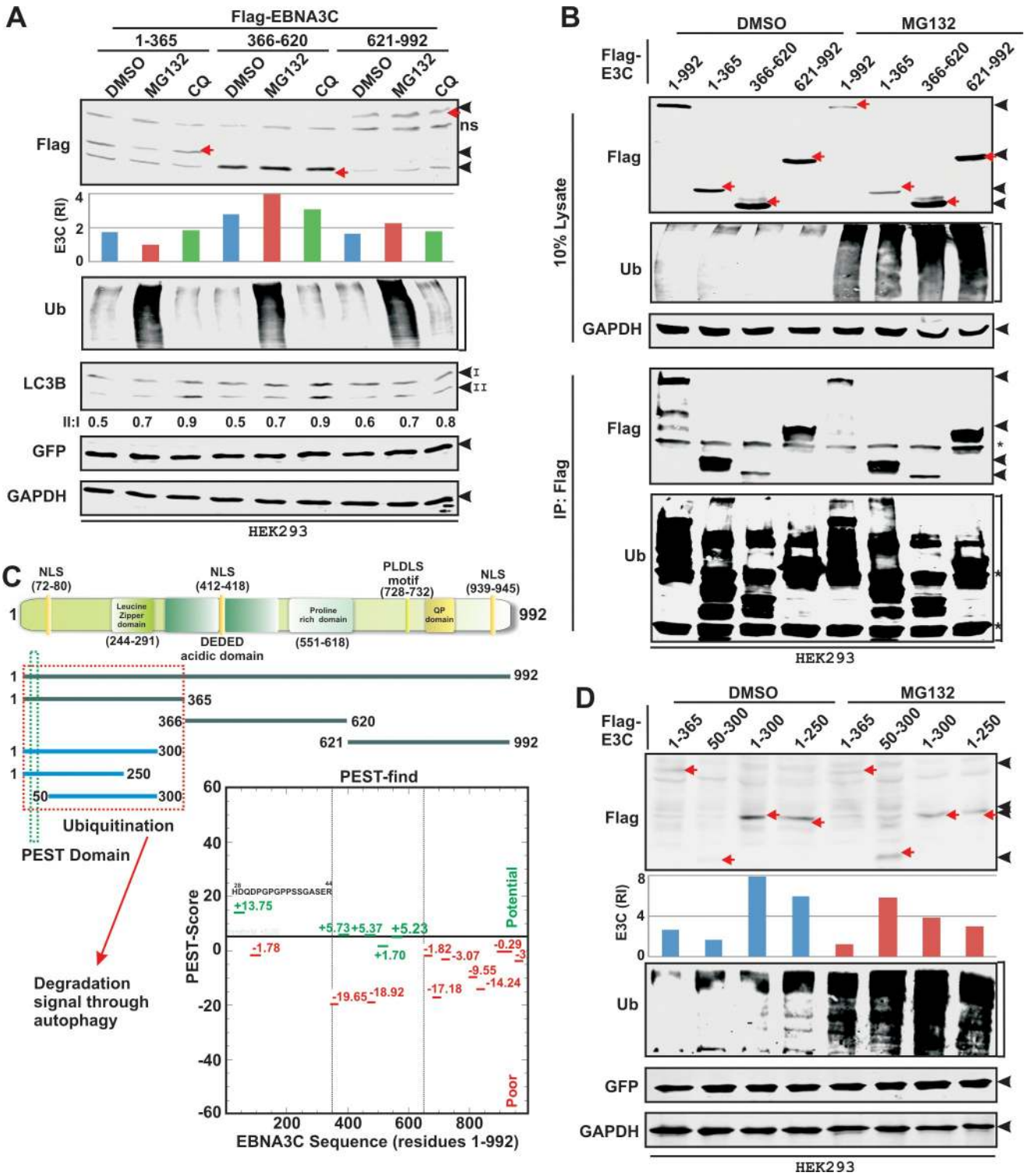

Fig 7. N-terminal domain of EBNA3C is important for autophagy mediated degradation in response to proteasomal inhibition. (A) HEK293 cells transiently transfected with plasmids expressing flag-tagged EBNA3C truncations–residues 1–365, 366–620 and 621–992, either left untreated (DMSO control) or treated with 20 μM MG132 or 50 μM Chloroquine (CQ), were harvested and subjected for western blot analyses with the indicated antibodies. (B) Using a similar experimental set up as described in (A), HEK293 cells transiently transfected with full-length (residues 1–992) and different domains of flag-tagged EBNA3C expression constructs, were subjected to immunoprecipitation (IP) with anti-flag antibody followed by western blot analyses with the indicated antibodies after stripping and reprobing the same membrane. (C) The schematic illustrates known structural motifs and different domains of EBNA3C that are used to determine residues important for autophagy mediated degradation upon proteasomal inhibition. Predicted PEST motifs were

derived by using http://emboss.bioinformatics.nl/cgi-bin/emboss/epestfind (green: potential; red: poor). (D) HEK293 cells transiently transfected with expression plasmids for flag-tagged EBNA3C N-terminal trunactions (residues 1–365, 50–300, 1–300 and 1–250) either were subjected to western blot analyses with the indicated antibodies after a similar treatment as described in (B). Protein band intensities in (A and D) were quantified by Odyssey imager software and indicated either as bar diagrams or LC3-II/I ratio at the bottom of each corresponding lane. Representative gel pictures are shown of two independent experiments. GAPDH and GFP blots were performed as loading and transfection efficiency controls, respectively.

https://doi.org/10.1371/journal.ppat.1008105.g007

cytoplasmic sections and upon MG132 treatment EBNA3C was specifically found to be degraded in the cytoplasmic fraction (Fig 8B). However, in contrast, p53 degradation occurred in the nuclear fraction in response to MG132 treatment (Fig 8B). The efficiency of subcellular fractionation was determined by GAPDH and lamin A/C blots as cytoplasmic and nuclear reference proteins, respectively (Fig 8B). To further correlate subcellular localization pattern and proteasomal inhibition mediated EBNA3C degradation, live-cell confocal microscopy analysis was carried out in HEK293 cells transiently transfected with GFP-tagged EBNA3C (Fig 8C). MG132 treatment resulted in co-localization of EBNA3C (wild-type, residues 1–992) with the lysosomal fraction in the cytoplasm (stained with LysoTracker Red DND-99) (Fig 8C).

Leptomycin B, an inhibitor of nuclear export, can cause the nuclear accumulation of proteins that shuttle between the cytosol and nucleus by targeting CRM1 (exportin 1), an evolutionarily conserved receptor for the nuclear export signal of proteins [58]. To further establish the role of nuclear export signal in mediating EBNA3C degradation in the cytoplasmic compartment, LCLs were treated with MG132 in the presence and absence of leptomycin B (20 ng/ml) and subjected for western blot and confocal analyses (Fig 8D and 8E, respectively). While leptomycin B treatment alone slightly enhanced EBNA3C expression in LCLs, it could not manage EBNA3C degradation induced by proteasomal inhibition (Fig 8D and 8E). The result suggests that EBNA3C degradation might occur in both nuclear and cytoplasmic compartments or leptomycin B failed to block cytoplasmic export of EBNA3C completely. The effect of leptomycin B was tested by conducting a fractionation experiment using HEK293 cells transiently transfected with flag-tagged EBNA3C with or without 24 h leptomycin B post-treatment (S6A Fig). The results demonstrated that leptomycin B treatment significantly enhanced (~3 fold) EBNA3C amount in nuclear fraction when compared to DMSO control (S6A Fig). The efficiency of fractionation was determined by western blot analyses against GAPDH as cytoplasmic protein and histone as nuclear protein (S6A Fig).

In order to determine whether both predicted NES sequences are functional or one of them are actively engaged in EBNA3C degradation upon proteasomal inhibition, GFP-tagged EBNA3C N-terminal (residues 1–365), C-terminal (residues 621–992) domains containing two putative NES sequences were utilized (Fig 8F–8I). Additionally, GFP-tagged EBNA3C middle part (residues 366–620) without any predicted NES sequence was also employed (S6B Fig). Live cell confocal experiments demonstrated that while the overall fluorescence intensity of N-terminal domain was drastically reduced particularly in the nuclear compartment, there was a significant increase in cytoplasmic translocation of C-terminal domain (compare Fig 8F and 8G). In contrast, as expected, no sign of cytoplasmic translocation was observed for the middle part (S6B Fig). Moreover, the results demonstrated that the puncta pattern of EBNA3C conferred by the C-terminal domain, while the N-terminal and middle regions presented rather a diffused pattern of fluorescence (Figs 8F, 8G and S6B). To get a clearer picture, subcellular fractionation was carried out in HEK293 cells transiently transfected with flag-tagged all three EBNA3C domains with or without MG132 treatment (Figs 8H, 8I and S6C). As similar to the full-length EBNA3C, both N-terminal and C-terminal domains were almost equally distributed in nuclear and cytoplasmic fractions, whereas the middle part exclusively present in the nuclear fraction (Figs 8H, 8I and S6C). The efficiency of subcellular fractionation was similarly validated by GAPDH and histone blots as cytoplasmic and nuclear reference proteins,

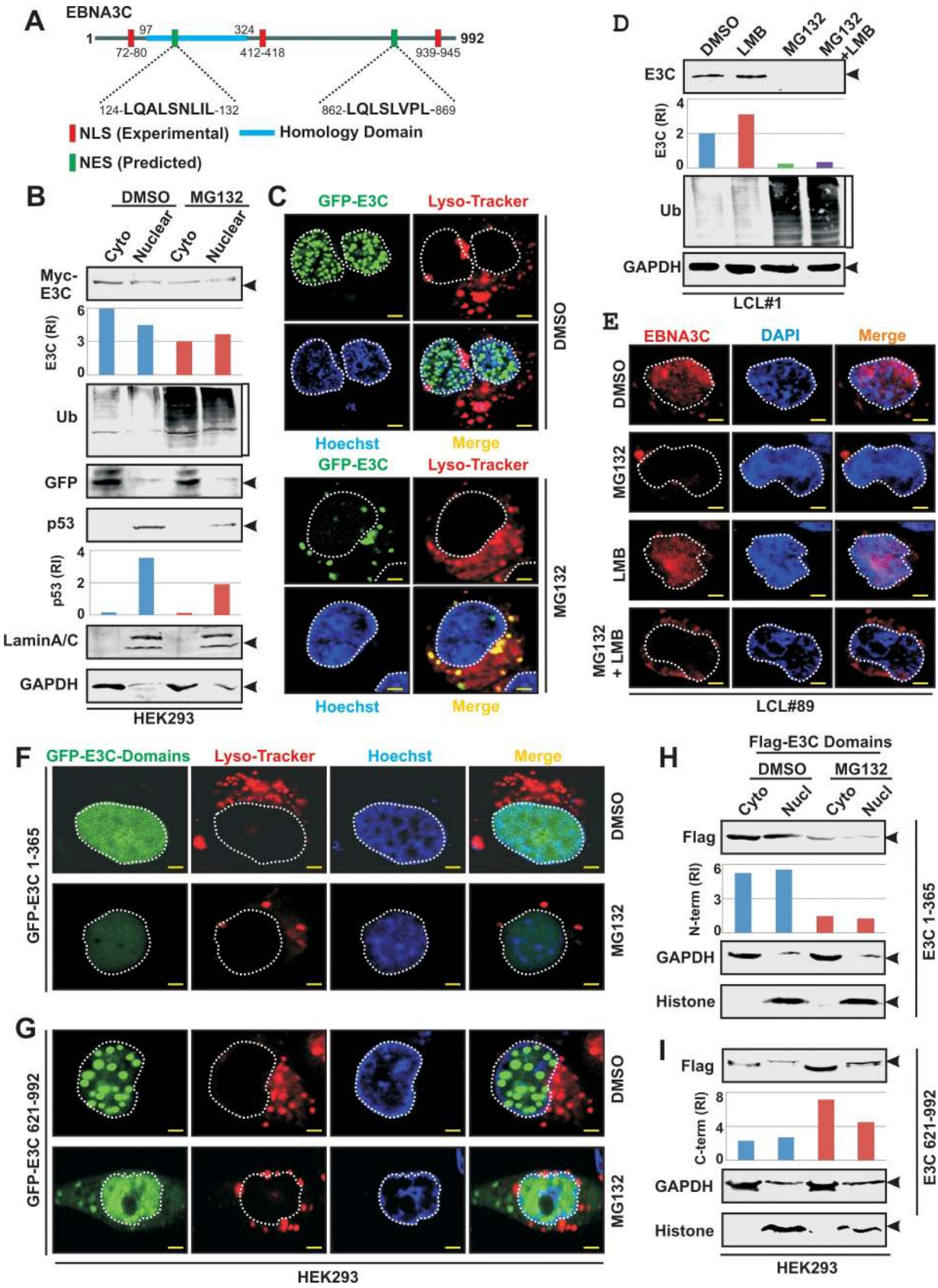
A
EBNA3C
1
97
324
992
72-80
412-418
939-945
124-LQALSNLIL-132
862-LQLSLVPL-869
NLS (Experimental)
Homology Domain
NES (Predicted)
B
DMSO
MG132
Cyto
Nuclear
Cyto
Nuclear
Myc-E3C
E3C (RI)
Ub
GFP
p53
p53 (RI)
LaminA/C
GAPDH
HEK293
C
GFP-E3C
Lyso-Tracker
Hoechst
Merge
DMSO
MG132
D
DMSO
LMB
MG132
MG132 +LMB
E3C
E3C (RI)
Ub
GAPDH
LCL#1
E
EBNA3C
DAPI
Merge
DMSO
MG132
LMB
MG132 + LMB
LCL#89
F
GFP-E3C-Domains
Lyso-Tracker
Hoechst
Merge
GFP-E3C 1-365
DMSO
MG132
G
GFP-E3C 621-992
DMSO
MG132
HEK293
H
Flag-E3C Domains
DMSO
MG132
Cyto
Nucl
Cyto
Nucl
Flag
N-term (RI)
GAPDH
Histone
E3C 1-365
I
Flag
C-term (RI)
GAPDH
Histone
E3C 621-992
HEK293

Fig 8. EBNA3C N-terminal domain is degraded in both nuclear and cytoplsamic fractions upon proteasomal inhibition. (A) Schematic shows the predicted nuclear export signal (NES) sequences of EBNA3C, derived from http://www.cbs.dtu.dk/services/NetNES/. (B-C) HEK293 cells were transiently transfected with the indicated expression plasmids. 36 h post-transfection cells were further treated with DMSO control or 20 μM MG132 for 4 h and subjected to (B) subcellular fractionation followed by western blot analyses using the indicated antibodies and (C) live cell confocal analyses. (D-E) LCLs were either left untreated (DMSO control) or treated with 0.5 μM MG132, 20 ng/ml leptomycin B (LMB) or MG132 plus LMB. 24 h post-treatment cells were subjected for either (D) western blot analysis or (E) immunostaining with the indicated antibodies. (C, F-G) Nuclei and lysosomes were counterstained with Hoechst 33342 and LysoTracker Red DND-99, respectively. Nuclei in (D) were counterstained by DAPI before mounting the cells. Each panel of confocal images in (C, E-G) is representative pictures of two independent experiments. Scale bars, 5 μm. (H-I) HEK293 cells transiently transfected with plasmids expressing flag-tagged EBNA3C N-terminal (residues 1–365) and C-terminal (residues 621–992) domains in a similar experimental set up as described in (B) were subjected to subcellular fractionation as per Manufacturer's instruction, followed by western blot analyses with the indicated antibodies. (B and H-I) GAPDH was used as reference protein for cytoplasmic fraction, while lamin A/C (B) and histone (H-I) blots were performed as nuclear reference proteins. Protein bands in (B, D, H-I) were quantified by Odyssey imager software and indicated as bar diagrams at the bottom of corresponding lanes.

https://doi.org/10.1371/journal.ppat.1008105.g008

respectively (Figs 8H, 8I and S6C). Quantification of the band intensities clearly indicated that MG132 treatment led to degradation of the N-terminal domain in both nuclear and cytoplasmic fractions, whereas the C-terminal domain was somewhat stabilized in both fractions (Fig 8H and 8I). In contrast, in accordance to our previous results the middle part appears to be unaffected in the nuclear fraction (S6C Fig). To further confirm the importance of NES sequences in regulating EBNA3C degradation upon proteasomal inhibition, live cell confocal microscopy was conducted using HEK293 cells transiently transfected with all three EBNA3C domains in the presence and absence of leptomycin B (S6D–S6F Fig). Although leptomycin B treatment did not have any influence on degradation pattern of EBNA3C domains, it significantly affected cytoplasmic translocation of the C-terminal domain as similar to the full-length protein induced upon proteasomal inhibition (S6D–S6F Fig). Taken together, the results suggest that nuclear export signal residing at both N- terminal and C-terminal domains play a crucial role for EBNA3C degradation in the cytoplasm through autophagy mechanism when proteasome is inhibited or overloaded due to accumulation of mis-/un-folded proteins.

Because the autophagy mediated proteolytic signal is located at the N-terminal region of EBNA3C (residues 1–50), to determine whether the N-terminal domain is also responsible for forming complex with autophagy components—p62/LC3B, an immunoprecipitation experiment was performed in HEK293 cells transiently transfected with either vector control or flag-tagged EBNA3C truncations–N-terminal (residues 1–365), middle part (residues 366–620) and C-terminal (residues 621–992) (S7A Fig). The results demonstrated that the only N-terminal domain bound to both p62 and LC3B (S7A–S7D Fig), which likely initiates EBNA3C degradation via autophagy-lysosomal pathway.

Caspases and reactive oxygen species do not affect proteasome inhibitor mediated degradation of EBNA3C

Studies suggest that caspases together with autophagy and UPS also contribute in proteolytic mechanisms particularly during apoptosis [19,59]. In addition, proteasome inhibitors have been shown to induce apoptotic cell death through the formation of reactive oxygen species (ROS) [59]. Apoptotic induction due to MG132 treatment, further prompted us to investigate whether caspases or ROS are involved in MG132 induced EBNA3C's degradation. However, no potential cut sites on EBNA3C's sequence were found for Caspases 1–10 using a web based peptide cutter tool (https://web.expasy.org/peptide_cutter/). Western blot results and confocal analyses also demonstrated that addition of a pan-caspase inhibitor, Z-VAD(OMe)-FMK could not rescue EBNA3C degradation in response to proteasomal inhibition (S8A and S8B Fig).

To evaluate the role of ROS in EBNA3C degradation N-acetyl-L-cysteine (NAC), a known ROS scavenger [60], was used and tested its ability to antagonize MG132 mediated ROS

generation in LCLs (S9A Fig). However, blocking the ROS by NAC did not restore EBNA3C expression as shown by both western blot and confocal analyses (S9B and S9C Fig). Overall, the data suggest that proteasomal inhibition mediated apoptotic induction and ROS had limited effect on modulation of EBNA3C expression. A similar result was also obtained for p53 degradation (S8A and S9A Figs).

Proteasome inhibitors can be used as potential therapeutic strategy against EBV associated B-cell lymphomas, where EBNA3C is expressed

Proteasome inhibitors specifically inhibit degradation of poly-ubiquitinated proteins through UPS, resulting in the stabilization of several tumor suppressor proteins that eventually promote cell-cycle arrest and apoptosis [61,62]. Previously it has been demonstrated that bortezomib, the first FDA approved proteasome inhibitor for the treatment of myeloma and mantle cell lymphoma, promotes EBV lytic cycle activation in Burkitt's lymphoma (BL) [52]. Induction of viral lytic replication in EBV transformed B-lymphocytes together with EBNA3C degradation upon proteasomal inhibition prompted us to evaluate proteasome inhibitors as a potential therapeutic strategy against EBV associated B-cell lymphomas where EBNA3C is expressed, particularly those are generated in an immunocompromised background. Soft agar based colony formation assays and cell viability experiments using trypan blue exclusion method on two LCLs (LCL#1 and LCL#89) demonstrated that both laboratory based and clinically approved proteasome inhibitors, MG132 and bortezomib, respectively, caused a significant reduction of total number of viable cells and colony formation ability in a dose dependent manner (Fig 9A–9D). Bortezomib (LD_{50}: ~0.5 **μ**M) showed approximately 10 fold higher cytotoxity than that of MG132 (LD_{50}: ~5 **μ**M) in LCLs (Fig 9D). To determine whether proteasomal inhibition caused apoptotic cell death, LCLs either left untreated (DMSO control) or treated with both MG132 (5 **μ**M) and bortezomib (0.5 **μ**M) for 24 h were stained with FITC labeled Annexin V in combination with propidium iodide (PI) and subjected for apoptosis analyses (Fig 9E). The results demonstrated that proteasome inhibition significantly induced apoptotic cell death in both LCLs (Fig 9E).

To determine whether proteasome inhibitors may exert different cytotoxic effects on B-cell lymphomas in respect to EBV infection status, cell viability assays was conducted in two EBV negative (BJAB and DG75) and two EBV positive (Namalwa and Raji) BL lines (S10A Fig). The results demonstrated that EBV positive lines both EBNA3C positive Namalwa and EBNA3C negative Raji cells as compared to EBV negative lines were somewhat more sensitive (~2 fold) to proteasome inhibitors induced cell death (S10A Fig), while an opposing effect was observed for autophagy inhibitors (S10B Fig). A similar trend of cell death in both EBNA3C negative line Raji and EBNA3C positive line Namalwa in response to proteasomal inhibition could possibly due to induction of viral lytic replication promoted by proteasome inhibitors as observed in LCLs (Figs 3B, 3D, S2B and S2D). EBNA3C expression was checked in different cell lines used in this study by western blot analyses (S10C Fig).

Previously we have shown that EBNA3C expression in EBV transformed B-lymphocytes significantly protects cell death induced by autophagy inhibitors [36]. Since EBNA3C was shown to enhance cytoprotective autophagy as well as block apoptosis in response to several cellular insults, similar cell viability assays were carried out in both EBNA3C stably expressing BJAB cells and EBNA3C knockdown LCLs to specifically determine if EBNA3C expression may influence proteasome inhibitors mediated cell death (Figs 10A and S11). The results demonstrated that while EBNA3C expressing B-cells as compared to the control line were more susceptible to cell-death induced by proteasome inhibitors in a dose dependent fashion, EBNA3C expression as expected led to a significant protection to cell death caused by

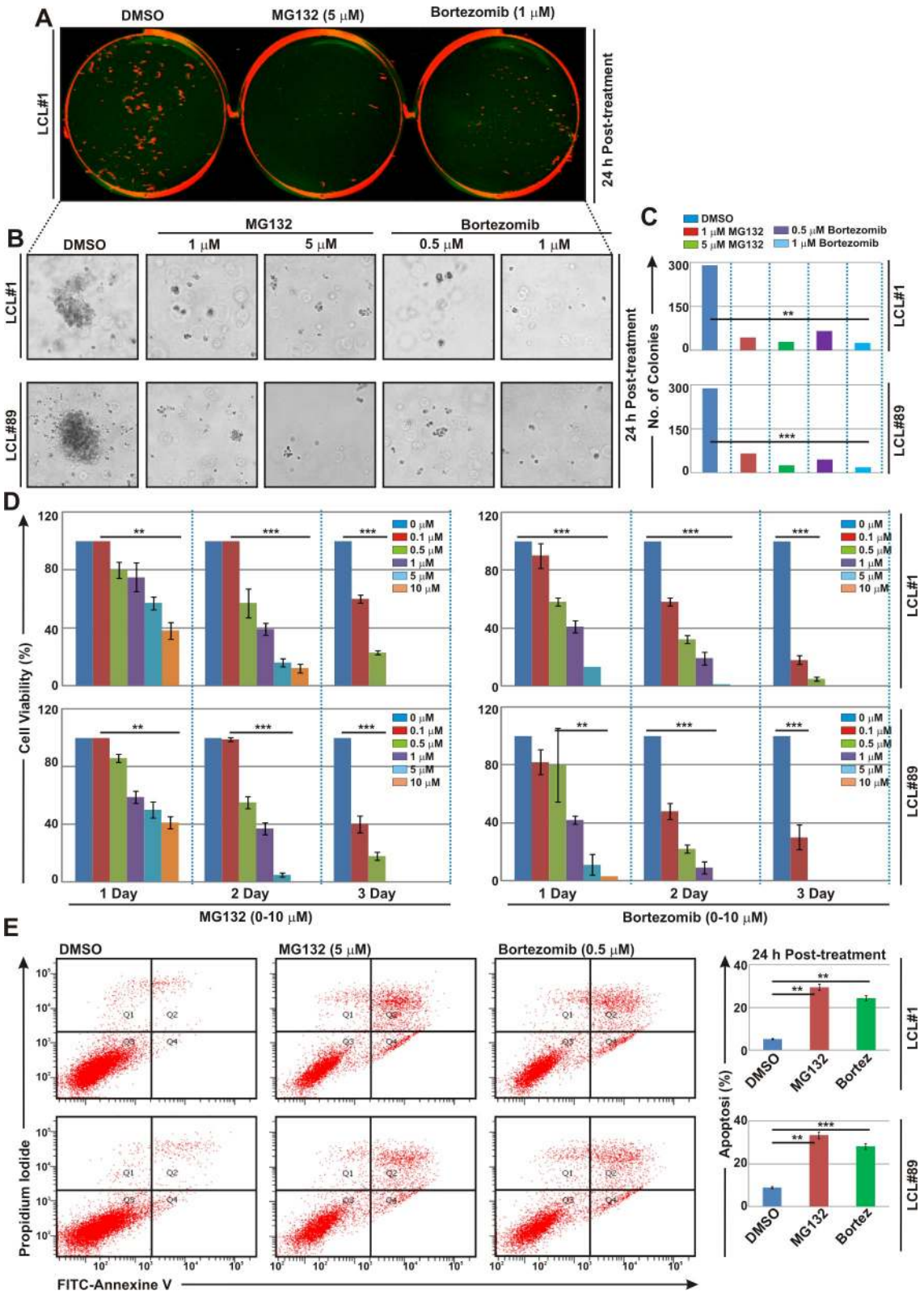

Fig 9. Proteasome inhibitors can be used as potential therapeutic strategy against EBV associated B-cell lymphomas. (A-C) 1×10^5 LCLs (LCL#1 and LCL#89) were either left untreated (DMSO control) or treated with increasing concentrations of MG132 (1–5 **μ**M) or bortezomib (0.5–1 **μ**M) for 24 h and subjected for soft agar colony formation assay as described in the "Materials and

Methods" section. After 14 days colonies were stained with 0.1% crystal violet and scanned using Odyssey CLx Imaging System and the number of colonies were measured by Image J software and plotted as bar diagrams in (C). Prior to staining, each well was also photographed (bright-field) using a Fluorescent Cell Imager as shown in (B). (D) ~0.5×10^5 LCLs (LCL#1 and LCL#89) plated into each well of six-well plates were either left untreated (DMSO control) or treated with increasing concentrations (0–10 μM) of MG132 or bortezomib for the indicated time points at 37˚C in a humidified CO_2 chamber. Viable cells from each well were measured by Trypan blue exclusion method using an automated cell counter. (E) ~0.5×10^5 LCLs (LCL#1 and LCL#89) plated into each well of six-well plates were either left untreated (DMSO control) or treated with 5 μM MG132 or 0.5 μM bortezomib for 24 h were subjected to apoptosis assay using annexin V/propidium iodide (PI) staining. FITC labeled annexin V binding (Ex = 488 nm; Em = 350 nm) and PI staining were detected using BD FACSAria III. Error bars represent standard deviations of duplicate assays of two independent experiments. *, **, *** = p-value < 0.01, 0.005 and 0.001 respectively.

https://doi.org/10.1371/journal.ppat.1008105.g009

autophagy inhibitors (Figs 10A and S11A and S11B). EBNA3C knockdown in LCLs reversed the effect of both proteasome and autophagy inhibitors (S11D and S11E Fig). EBNA3C stable expression in BJAB and knockdown in LCLs were checked by western blot analyses (S11C and S11F Fig, respectively). Susceptibility of proteasomal inhibitors mediated cell death in EBNA3C expressing B-cells was further validated by apoptosis, PARP cleavage and soft agar colony formation assays (Fig 10B–10D). The results confirmed that as compared to control cells, EBNA3C expression led to increased cell apoptosis, PARP cleavage and reduced colony formation ability in response to both proteasome inhibitors (Fig 10B, 10C and 10D, respectively). Overall, the data show promise for proteasome inhibitors as anti-cancer drugs against multiple EBV associated B-cell lymphomas where EBNA3C is expressed (Fig 11).

Discussion

EBNA3 family proteins consisting of EBNA3A, EBNA3B and EBNA3C are three closely related EBV nuclear proteins that are expressed only in latency III associated B-cell lymphomas and *in vitro* transformed continually proliferating LCLs [13,14]. Genetic analysis using recombinant viruses has shown that EBNA3A and EBNA3C, but not EBNA3B, are essential for B-cell activation and subsequent immortalization *in vitro* [8,9,45]. Previously, these EBNA3 proteins were shown to be extremely stable in growing LCLs, although *in vitro* they interact with 20S proteasome, one of the major proteolytic components of 26S proteasome in ubiquitin-proteasome system (UPS) of eukaryotic cells [33]. 26S proteasome, a 2.5-MDa self-compartmentalized proteolytic machine located in the cytosol and nucleus, comprises of two 19S regulatory particles responsible for recognition of poly-ubiquitinated proteins marked for proteolytic degradation, assemble each end of the barrel-shaped 20S proteasome, where proteolysis takes place [63]. In eukaryotic cells, UPS is considered as one of the key protein degradation mechanisms, affecting an array of important cell pathways [20,21]. Consequently, specific chemical inhibitors of UPS have recently emerged as attractive anticancer drugs [61,62]. For example, bortezomib (Velcade) has been approved by the US Food and Drug Administration (FDA) as the first proteasome inhibitor for the treatment of refractory multiple myeloma and mantle cell lymphoma [48,64].

Proteasome function can be hindered in many ways. For example, cancer cells for its high metabolic activity often encounter ER stress due to accumulation of misfolded and aggregated proteins exerting an unfolded protein response (UPR) [65]. Such protein aggregates can bind and stabilize an inactive closed conformation of the 26S proteasome [66]. Additionally, UPS alone is not capable enough to alleviate UPR and resulting in apoptotic cell death. Thus, in order to survive and properly function, cells must obliterate these protein aggregates, where autophagy-lysosomal pathway comes into the picture as a compensatory proteolytic mechanism particularly when proteasome function is inhibited [67,68]. In agreement to this, a growing body of evidence demonstrates proteasomal inhibition can promote degradation of a number of important cellular proteins thorough activating autophagy mechanism. For

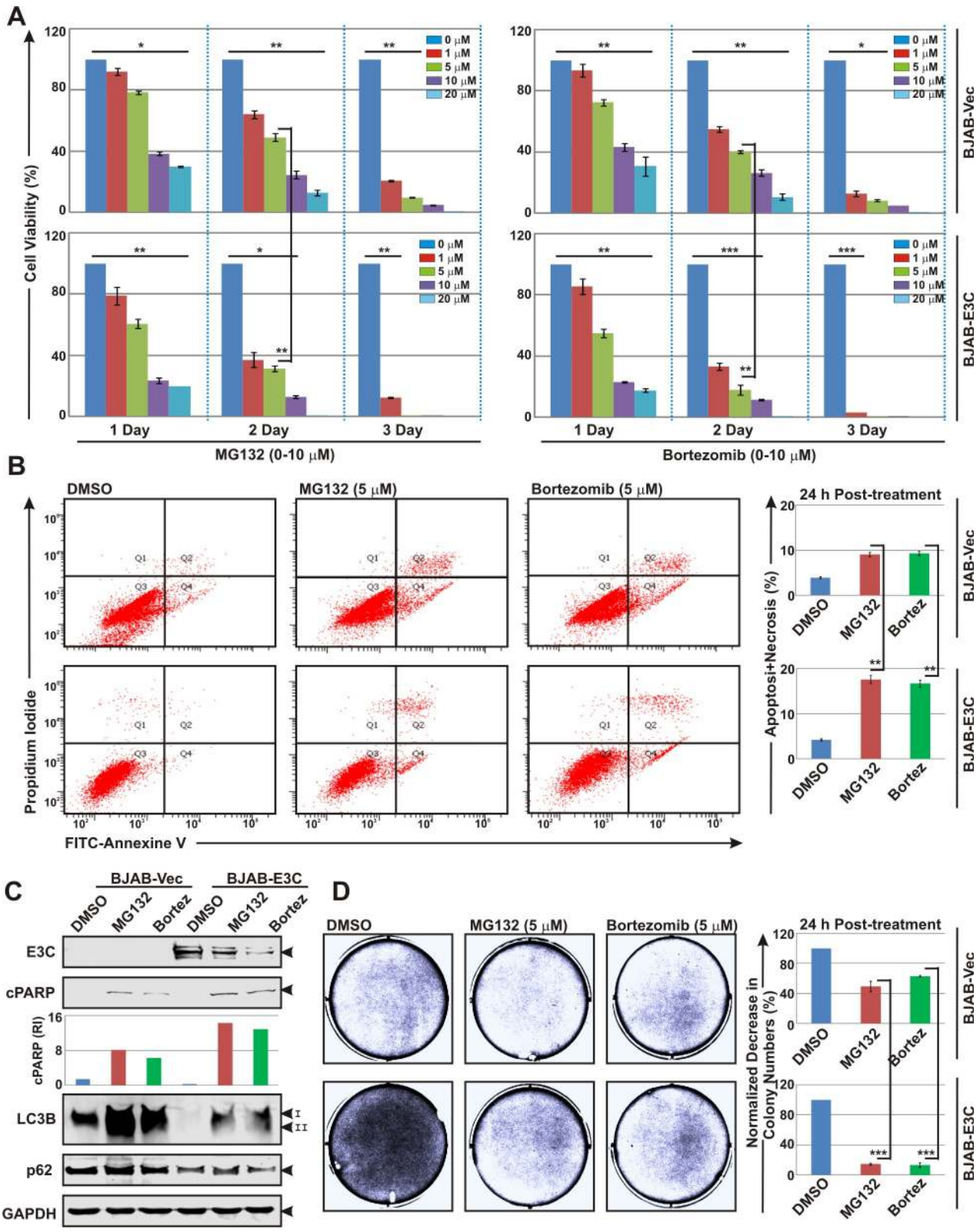

Fig 10. EBNA3C expressing B-cells are more sensitive to apoptotic cell death induced by proteasome inhibitors. (A) ~0.5 × 10^5 BJAB cells stably harboring vector or EBNA3C expressing plasmid plated into each well of six-well plates were either left untreated (DMSO control) or treated with increasing concentrations (0–20 μM) of MG132 or bortezomib for 3 days. Viable cells from each well were measured by Trypan blue exclusion

method using an automated cell counter. (B-D) ~10 × 10^5 BJAB-vector or BJAB-EBNA3C cells were treated with DMSO, or 5 μM of MG132 or bortezomib for 24 h were subjected to (B) apoptosis assay using annexin V/propidium iodide (PI) staining, (C) western blot analyses using indicated antibodies and (D) soft agar colony formation assay as described in the "Materials and Methods" section. GAPDH blot was used as loading control in western blot analyses. Protein bands were quantified by Odyssey imager software and indicated as bar diagrams at the bottom of corresponding lanes. Error bars represent standard deviations of duplicate assays of two independent experiments. *, **, *** = p-value < 0.01, 0.005 and 0.001 respectively.

https://doi.org/10.1371/journal.ppat.1008105.g010

example, it has been shown that while wild-type p53 is stabilized by autophagy activation, oncogenic mutant p53 is degraded by autophagy-lysosomal pathway in response to proteasomal inhibition in breast cancer cell lines [37]. Other examples of cell oncoproteins that are degraded through autophagy include the two fusion oncoproteins—BCR-ABL and PML-RARA, anterior gradient 2 (AGR2), a member of the protein disulfide isomerase (PDI) family, and cyclin dependent kinase 1 (CDK1) [38,69,70,71]. In addition, JC virus (JCV) encoded large T-antigen was shown to be degraded through autophagy mediated by Bag3, a member of the Bcl-2-associated athanogene (Bag) family of proteins [72]. Current knowledge about the role of autophagy in regulating expressions of EBV encoded oncoproteins is

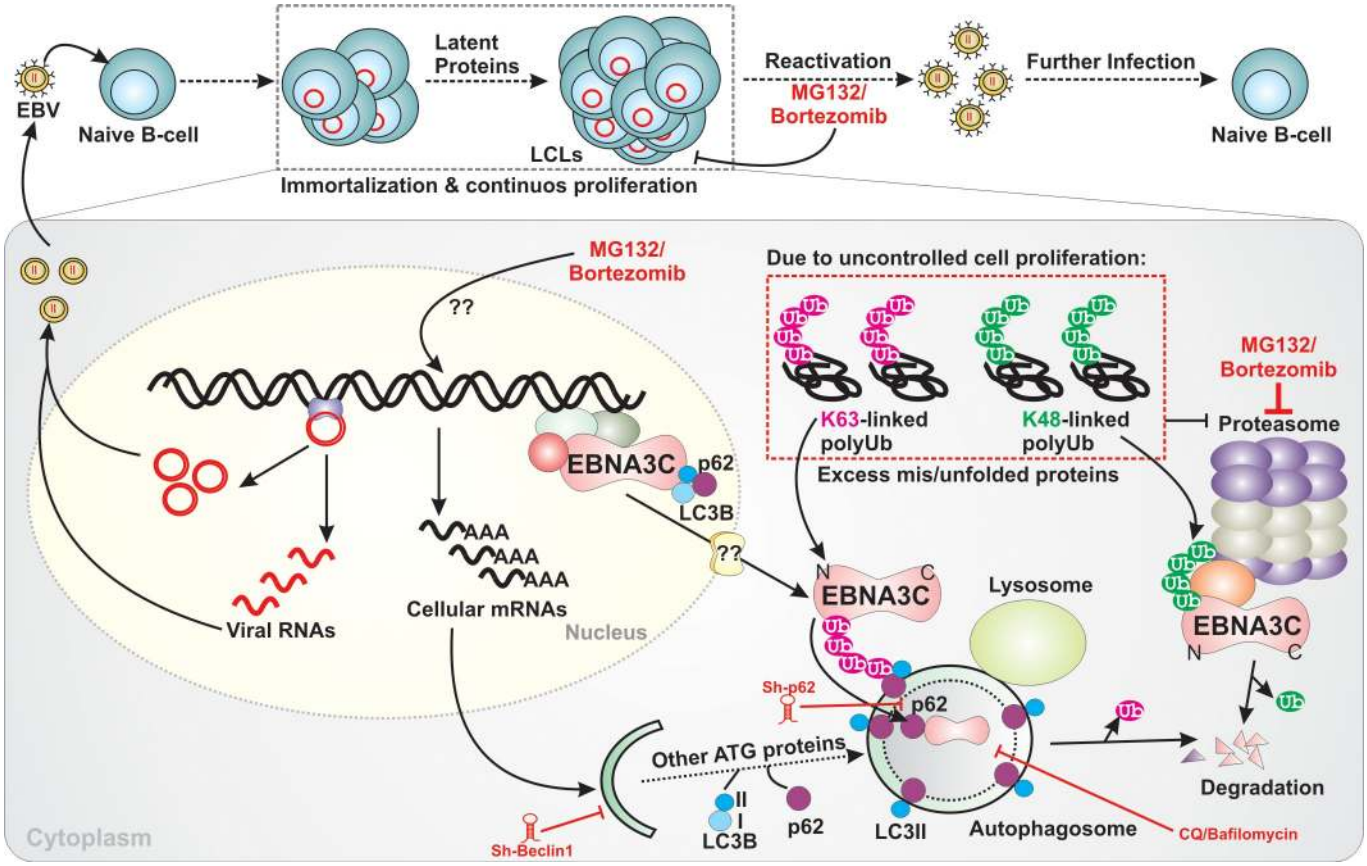

Fig 11. Schematic representation of proteasomal inhibition mediated EBNA3C's degradation. Due to uncontrolled cell proliferation, cancer cells often encounter excess mis-/un-folded protein aggregates, which are subsequently labeled with either K48-linked or K63-linked polyubiquitination for proteolytic degradation. While K48-linked ubiquitin chains are targeted for the proteasomal pathway, K63-linked directs autophagy mediated protein degradation. Upon proteasomal inhibition, EBV oncoprotein EBNA3C is predominantly tagged with K63-linked polyubiquitin chains, translocated to cytoplasm by an unknown mechanism and degraded through autophagy-lysosomal pathway. The N-terminal domain plays a central role in EBNA3C's degradation through autophagy mechanism by participating within the p62-LC3B complex. Suppression of autophagy pathway (Beclin1 and p62 knockdown or chloroquine (CQ)/bafilomycin treatment) reverses EBNA3C degradation in response to proteasomal inhibition. Additionally, proteasomal inhibitors (such as MG132) induce both autophagy and viral gene transcription that eventually activate viral lytic replication. The results provide foundation to exploit proteasome inhibitors as potential therapeutic approach for EBV associated B-cell lymphomas, where EBNA3C is expressed, typically diagnosed in immunocompromised individuals.

https://doi.org/10.1371/journal.ppat.1008105.g011

primarily limited to EBNA1 and LMP1. While LMP1 modulates autophagy pathway to regulate its own degradation, EBNA1 is degraded through autophagy-lysosomal pathway for MHC class II mediated antigen presentation [34,47]. Thus, the available data are consistent with a notion that disruption of autophagy function can act as a tumor barrier through degradation of both cell and viral oncoproteins in response to various cellular insults.

In this report, for the first time we show that proteasomal inhibition enhances degradation of a viral oncoprotein, EBV encoded essential oncoprotein EBNA3C through autophagy-lysosomal pathway (Fig 10). Although share a considerable structural similarities [16], proteasomal inhibition causes degradation of only two EBNA3 family members oncoproteins–EBNA3A and EBNA3C, but not the third member–the viral tumor suppressor protein EBNA3B. Recently we have shown that EBNA3C enhances the basal level of autophagy, which serves as a prerequisite for EBNA3C mediated cell proliferation and apoptotic inhibition [36]. In the absence of growth promoting signals this autophagy activation is further enhanced through engaging an epigenetic regulation [36]. It is not entirely clear to what extent basal autophagy contributes to EBNA3C degradation, while autophagic disruption arises when autophagy is stimulated higher than the basal levels in response to stress signals (including UPR or starvation) or drug treatment (such as proteasome inhibitors). As discussed above, autophagy can also be induced in response to a heavy burden of aggregated proteins [67,68]; in our model autophagy induction alone was unable to induce EBNA3C degradation. Dual treatment with inhibitors of the UPS (MG312) and autophagy (chloroquine or bafilomycin) or ablation of autophagy pathway by sh-RNA mediated Beclin1 or p62 knockdown revealed that autophagy-lysosomal pathway plays a crucial role in degradation of EBNA3C (and possibly along with other protein aggregates) caused by UPS inhibition. Our data also indicate that autophagy inhibition could not fully compensate EBNA3C expression caused by UPS impairment. Interestingly, it has earlier been shown that basal but not enhanced autophagy activity regulates UPS mediated Sirt3 degradation in chronic myeloid leukemia cells [73]. This offers an adaptive mechanism by which autophagy in association with UPS mitigates oxidative stress in the leukemia cells.

Earlier, we have demonstrated that EBNA3C expression increases basal level of K63-linked polyubiquitination, which further increases in absence of growth promoting signals [36]. Additionally, EBNA3C was shown to recruit UPS to regulate turn-over of many important cell oncoproteins and tumor suppressors [27,28,29,30,31,74,75,76]. Initially Knight et al. demonstrated the poly-ubiquitination on the N-terminal domain of EBNA3C [28]. However, the authors conducted the study in native conditions and thus cannot rule out the possibility of association of other ubiquitinated proteins within the complex. In this study, using immunoprecipitation under denaturing conditions we now show for the first time that EBNA3C are specifically covalently tagged by K63-linked polyubiquitin chains. Ubiquitin chains with these different linkages are thought to direct proteins towards different fates owing to the specificity of binding partners for specific lysine-linkages. While K48-linked polyubiquitin chains are coupled with proteasome mediated degradation, K63-linked chains direct degradation of substrate protein through autophagy-lysosomal pathway [54,55]. The presence of K63-chain on EBNA3C offers a model in which K63–ubiquitin labeled EBNA3C is targeted for proteolytic degradation through autophagy-lysosomal pathway. The autophagic adaptor protein p62/SQSTM1 selectively binds to K63-linked polyubiquinated chains and subsequently recruits to LC3-positive autophagosomes for degradation [23,55]. Our data also reveals that EBNA3C forms a stable complex with p62/LC3B. Bioinformatics analyses could not however reveal any putative LIR (LC3 interacting region) domain in EBNA3C [24,77], suggesting that EBNA3C perhaps does not directly bind to LC3B. The interaction may occur through p62 and K63-polyubiquition linked EBNA3C.

The N-terminal domain of EBNA3C is of particularly interesting, at least in the context of interacting with plethora of important cell proteins particularly involved in cell-cycle activation and blockade of apoptosis [14,30,31,74,76,78,79,80]. Interestingly, many of these proteins' turn over or stability is deregulated through UPS specifically recruited by the N-terminal domain of EBNA3C. For example, EBNA3C enhances degradation of $p27^{KIP1}$ and p53 tumor suppressor proteins through recruiting SCF^{Skp2} and Mdm2 E3 ligase activities, respectively and thereby promoting EBV induced B-cell lymphomagenesis [28,30]. Moreover, using genetic engineering the N-terminal residues were shown to be essential for survival of EBV transformed B-lymphocytes [81]. Our results demonstrate that this N-terminal domain (residues 1–365) participates within the p62-LC3B complex and particularly the first 50 residues of EBNA3C comprising a putative PEST domain is responsible for autophagy mediated degradation upon proteasomal inhibition. This supports a model whereby the N-terminal domain plays a feedback mechanism to control EBNA3C expression through autophagy-lysosomal pathway in response to proteasomal impairment. The presence of putative nuclear export signal (NES) sequences in both N- and C-terminal domains also indicate a possible mechanism of EBNA3C degradation through autophagy in the cytoplasmic fraction. In fact, our results demonstrate that MG132 treatment leads to EBNA3C's degradation in both nucleus and cytoplasm. However, the precise mechanism by which EBNA3C shuttles between nucleus and cytoplasm in response to proteasomal inhibition is yet to be defined. Although extensive studies have focused on autophagic turnover of cytoplasmic materials, little is known about the role of autophagy in degrading nuclear components. Recent studies have highlighted the importance of nuclear autophagy in both physiological and pathological processes, such as cancer [82,83]. LC3B is present in the nucleus and directly interacts with the nuclear lamina protein lamin B1. Importantly, this LC3B-lamin B1 interaction does not downregulate lamin B1 during starvation, but mediates its degradation upon oncogenic insults, such as by activated RAS. Lamin B1 degradation is achieved by nucleus-to-cytoplasm transport that delivers lamin B1 to the lysosome [83]. As discussed above, oncogenic mutant p53 has been shown to be degraded through autophagy-lysosomal pathway when proteasome is inhibited [37]. However, it is still unclear whether p53 is degraded in the nuclear or cytoplasmic fraction. Moreover, previously it has been demonstrated that in response to multiple DNA damages p53 could be degraded in both cytoplasm and nuclear fraction [84]. In spite of nuclear export blockade, p53 degradation occurs locally in the nucleus, in parallel to cytoplasmic degradation [84]. In agreement to this, our results demonstrate that in contrast to EBNA3C, p53 is specifically targeted in the nuclear compartments for degradation when proteasome is inhibited.

Previously, proteasome inhibitors, such as MG132 have been demonstrated to exert substantial protective effect on cardiovascular and renal injury and appear to be potentially effective drugs in blocking oxidative damage as well as increased atherosclerosis in rabbits [85,86,87,88]. MG132 treatment was shown to enhance clearance of nuclear progerin protein through autophagy and regulating splicing mechanisms by downregulating SRSF-1 [39]. Besides its proteolytic functions, proteasomal machinery also provides non-proteolytic activities engaging transcriptional and post-transcriptional regulation of multiple cellular genes [39,69,89]. In agreement to this, our RNA-seq data reveals that proteasomal inhibition enhances transcriptional activation of genes (viz. MAP1LC3B, p62/SQSTM1 and GABARAPL1) involved in autophagosome formation. Moreover, in contrast to proteolytic degradation of EBNA3 proteins, proteasomal inhibition results in transcriptional activation of both EBV latent including the EBNA3 family genes and lytic genes, which subsequently promotes viral lytic cycle. As a result as compared to EBV negative lines, EBV positive cells were shown to more sensitive to cell death induced by proteasome inhibitors possibly due to production of infectious virus particles. There is a growing interest in pharmacologic activation of lytic viral

gene expression as a potential therapeutic strategy against several virus associated human cancers [50]. Of note, it has been earlier demonstrated that bortezomib treatment augments EBV lytic cycle activation in Burkitt's lymphoma cell lines [52]. The authors suggested that UPR regulator CCAAT/enhancer-binding protein (CEBPβ), a member of the bZIP family of transcription factors, transcriptionally activates BZLF1 or ZTA expression that eventually controls EBV lytic cycle activation [52]. In this line, our lab is currently investigating the role of UPR activators in EBNA3C degradation as a prospective therapeutic option. Altogether these results suggest that proteasome inhibitors can have encouraging therapeutic effects without having any potential cytotoxicity.

In conclusion, herein the results provided the basis for the development of novel class of drug against multiple EBV linked B-cell lymphomas, expressing EBNA3 family proteins. We provided evidence that proteasomal inhibition specifically promotes degradation of two viral oncoprotein EBNA3A and EBNA3C through autophagy-lysosomal pathway along with induction of viral lytic cycle. A new promising path hence begins for therapeutic development of proteasome inhibitors (such as bortezomib) in combination with EBV replication inhibitors (such as Ganciclovir) toward a better treatment in near future for patients affected with EBV associated B-cell lymphomas particularly those generated in an immunocompromised background.

Materials and methods

Drugs

MG132 (ab141003), bortezomib (ab142123) and Z-VAD(OMe)-FMK (ab120487) were obtained from Abcam (Cambridge, UK). Chloroquine diphosphate salt (C6628), Cycloheximide (C7698), Leptomycin B (L2913), N-Acetyl-L-cysteine (A9165), Doxycycline hyclate (D9891), G418 sulfate (345810), 12-O-Tetradecanoylphorbol-13-acetate or TPA (P1585), sodium butyrate (B5887), Polybrene (TR-1003-G) and Puromycin dihydrochloride (P8833) were brought from Sigma-Aldrich Corp. (St. Louis, MO, USA).

Plasmids

Myc-, flag-, GFP- and RFP-tagged EBNA3C constructs in pA3M, pA3F, pEGFP-C1 and pDsRED-Monomer-N1 vectors, respectively were previously described [27,29,36]. Myc-tagged EBNA1 expressing construct in pA3M was described earlier [90]. Myc- and flag-tagged EBNA3C truncation constructs expressing EBNA3C residues 1–365, 366–620 and 621–992 were previously described [27,29]. Myc-tagged EBNA3C N-terminal residues 1–365 expressing construct was used as a template for preparing three more EBNA3C truncations–residues 1–300, 1–250 and 50–300 in pA3M (pCDNA3.1-3X Myc) at *Eco*RI and *Not*I restriction sites. pA3M-EBNA3C construct was used as a template to clone GFP-tagged EBNA3C truncation constructs expressing residues 1–365 and 621–992 in pEGFP-C1 vector at *Eco*RI and *Sal*I restriction sites. All the constructs were further verified by Sanger dideoxy based DNA sequencing (Eurofins Genomics India Pvt. Ltd., India). pEGFP-C1 and pDsRED-Monomer-N1 plasmids were obtained from Clontech Laboratories, Inc. mCherry-tagged p62 expressing plasmid was a kind gift from Edward M. Campbell (Loyola University Chicago, IL, USA). pBabePuro-GFP-LC3 construct was a kind gift from Jayanta Debnath (Addgene plasmid# 22405). pTripz-mCherry-Sh-Beclin1 construct (Clone ID: V2THS_23692) was obtained from GE Healthcare Dharmacon Inc. (Lafayette, CO, USA). pGipz-Sh-Control and pGipz-Sh-EBNA3C were previously described [36]. Lentiviral packaging vectors—pCMV-VSV-G (Addgene plasmid# 8454), pRSV-Rev (Addgene plasmid# 12253), and pMDLg/pRRE (Addgene plasmid# 12251) were kind gifts from Robert A. Weinberg (Whitehead Institute for Biomedical research, Cambridge, MA, USA).

Antibodies

Mouse monoclonal antibody against EBNA3C (A10) generated from hybridoma cells was previously described. Sheep polyclonal antibodies against EBNA3A (ab16126), EBNA3B (ab16127) and EBNA3C (ab16128) were bought from Abcam (Cambridge, UK). Rabbit polyclonal anti-GFP (ab290), rabbit anti-Sheep IgG (H+L), rabbit polyclonal anti-Histone H3 (ab1791) and rabbit monoclonal anti-LMP1 (ab136633) antibodies were also obtained from Abcam (Cambridge, UK). Mouse monoclonal antibodies directed against p62/SQSTM1 (Clone# 3/P62 lck ligand), Beclin1 (Clone# 20/Beclin), cleaved PARP (Clone# Asp214), total ubiquitin (Clone# 6C1.17) were purchased from BD Biosciences (Franklin Lakes, NJ, USA). Rabbit monoclonal antibodies directed against LC3A/B (Clone# D3U4C), K48-linkage specific polyubiquitin (D9D5) and K63-linkage specific polyubiquitin (D7A11) were purchased from Cell Signaling Technology Inc. (Danvers, MA, USA). Mouse monoclonal anti-flag (M2) and anti-cMyc (9E10) antibodies were purchased from Sigma-Aldrich Corp. (St. Louis, MO, USA). Mouse monoclonal anti-MDM2 (SMP14), anti-p53 (DO-1) and anti-GAPDH (0411) antibodies were purchased from Santa Cruz Biotechnology, Inc. (Dallas, TX, USA). Rabbit polyclonal antibody against Lamin A/C (NB100-56649) was obtained from Novus Biologicals, LLC (Centennial, CO, USA). DyLight 800/680 conjugated (for western blots) and Alexa Fluor 488/555 tagged (for confocal micoscopy) secondary antibodies anti-mouse, anti-rabbit, anti-sheep IgG (H+L) were purchased from Thermo Fisher Scientific Inc. (Waltham, MA, USA).

Cell lines and cell culture

HEK293 cells were obtained from Rupak Dutta (Indian Institute of Science Education and Research, Kolkata, India). HEK293T cells were purchased from GE Healthcare Dharmacon Inc., Lafayette, CO, USA. Both HEK293 and HEK293T cells were maintained in Dulbecco's modified Eagle's medium (DMEM) (Gibco/Invitrogen, Inc., USA) supplemented with 10% fetal bovine serum (FBS) (Gibco/Invitrogen, Inc., USA), 1% Penicillin-Streptomycin Solution (Sigma-Aldrich Corp., St. Louis, MO, USA). EBV-positive Burkitt's lymphoma (BL) cell line Namalwa was obtained from National Centre for Cell Science, (NCCS, Pune, Govt. of India). EBV-negative BL lines–DG75, BJAB and BJAB stably expressing EBNA3A and EBV positive BL line Raji cells were obtained from Elliott Kieff (Harvard Medical School, USA). *In vitro* EBV transformed LCL clones (LCL#1 and LCL#89), EBV-negative BL line BJAB, BJAB clones stably expressing either vector or EBNA3C cDNA (E3C#7) and lentivirus-mediated stable EBNA3C knockdown (LCL#Sh-E3C) or control (LCL#Sh-Con) lymphoblastoid cell lines (LCLs) were previously described [36]. LCL#Sh-E3C and LCL#Sh-Con cells were freshly generated in LCL#1 as described below. BJAB-vector and BJAB-EBNA3C cells were maintained in complete RPMI media supplemented with 500 μg/ml G418 (Sigma-Aldrich Corp., St. Louis, MO, USA). LCL#sh-control and LCL#sh-EBNA3C cells were maintained in complete RPMI media supplemented with 1 μg/ml puromycin (Sigma-Aldrich Corp., St. Louis, MO, USA). LCLs were maintained in RPMI 1640 (Gibco/Invitrogen, Inc., USA) supplemented with 10% FBS and 1% Penicillin-Streptomycin Solution. Unless otherwise stated all above-mentioned cells were cultured at 37˚C in a humidified environment supplemented with 5% CO_2.

Western blotting

Unless and otherwise stated, ~10 x 10^6 adherent or B-cells were harvested, washed with ice cold 1X PBS (Invitrogen, Thermo Fisher Scientific Inc., Waltham, MA, USA), and subsequently lysed in 0.5ml ice cold RIPA buffer (Sigma-Aldrich Corp., St. Louis, MO, USA) with protease inhibitor cocktail (Cell Signaling Technology Inc., Danvers, MA, USA). Protein concentrations were estimated by Bradford reagent (BIO-RAD, Hercules, CA, USA). Samples

were boiled in 2 X laemmli buffer (BIO-RAD, Hercules, CA, USA), fractionated by SDS-PAGE and transferred to a 0.45 μm either nitrocellulose or low autofluorescence PVDF membranes (BIO-RAD, Hercules, CA, USA). The membranes were then probed with specific antibodies followed by incubation with appropriate infrared-tagged/DyLight secondary antibodies and viewed on an Odyssey CLx Imaging System (LiCor Inc., Lincoln, NE, USA). Image analysis and quantification measurements were performed using the Odyssey Infrared Imaging System application software (LiCor Inc., Lincoln, NE, USA).

Transfection

Unless and otherwise stated, ~10 x 10^6 HEK293 cells were harvested, resuspended with 450 μL Opti-MEM medium (Invitrogen, Thermo Fisher Scientific Inc., Waltham, MA, USA), mixed with appropriate plasmids in a 0.4-cm gap cuvette (BIO-RAD, Hercules, CA, USA) and transfection was performed by electroporation using a Gene Pulser II electroporator (BIO-RAD, Hercules, CA, USA) at 210 V and 975 μF for Western Blot analyses. Cells were harvested 36 h post-transfection for western blot analyses, unless and otherwise stated. For confocal microscopy, cells were transfected with appropriate plasmids using Lipofectamine 3000 according to manufacturer's protocol (Invitrogen, Thermo Fisher Scientific Inc., Waltham, MA, USA). 24 h post-transfection cells were subjected to live-cell confocal microscopy analyses.

Stability assay

~5 x 10^6 EBV transformed B-lymphocytes (LCL#1) or EBNA3C stably expressing BJAB cells (BJAB-E3C#7) were treated with 100 μg/ml cyclohexamide (Sigma-Aldrich Corp. St. Louis, MO, USA) alone (with DMSO control) or in the presence of 1 μM MG132 (Abcam Inc, Cambridge, UK) or 50 μM Chloroquine (Sigma-Aldrich Corp. St. Louis, MO, USA) in normal growth medium for 24 h. Subsequently, lysates were prepared in 1 x RIPA buffer at indicated time periods and subjected to western blot analyses with appropriate antibodies. Band intensities were quantified by Odyssey imager (LiCor Inc., Lincoln, NE, USA).

Confocal microscopy

~1 x 10^6 HEK293 cells grown at 70% confluency on 35 mm dish embedded with 12 mm glass viewing area (Nunc, Thermo Fisher Scientific Inc., Waltham, MA, USA) were transfected with appropriate plasmids using Lipofectamine 3000. 24 h post-transfection cells were either left untreated (DMSO control) or treated with 20 μM MG132 for another 4–6 h and subsequently subjected for live-cell confocal analyses. For live-cell imaging, Hoechst 3342 solution (Thermo Fisher Scientific Inc., Waltham, MA, USA) and LysoTracker Red DND-99 (Invitrogen, Thermo Fisher Scientific Inc., Waltham, MA, USA) were used to stain the nucleus and the acidic lysosomes, respectively. For LCLs, approximately 1 million cells either left untreated (DMSO control) or treated with 1 μM MG132 for 12 h were harvested in microcentrifuge tubes, washed with 1 X PBS, fixed and permeabilized with 4% paraformaldehyde (Sigma-Aldrich Corp. St. Louis, MO) and 0.1% Triton X-100 (Sigma-Aldrich Corp. St. Louis, MO, USA) followed by blocking with 5% BSA (BIO-RAD, Hercules, CA) at room temperature for 1 h. Cells were further incubated with appropriate primary antibodies for overnight at 4˚C. Nucleus was counterstained with 4', 6',-diamidino-2-phenylindole (DAPI; BIO-RAD, Hercules, CA, USA) for 30' at room temperature. Alexa Fluor labeled secondary antibodies diluted in blocking buffer (1:2000) were incubated at room temperature for another 1 h. Cells were then washed for three times with 1 X PBS and mounted using an antifade mounting media (Sigma-Aldrich Corp. St. Louis, MO, USA) in 8-well chamber slides (Thermo Fisher Scientific Inc., Waltham, MA, USA) for confocal microscopy. The images were obtained by a Leica

DMi8 Confocal Laser Scanning Microscope and analyzed in the Leica Application Suite X (LAS X) software (Leica Microsystems GmbH, Wetzlar, Germany). The intensities of stains were sometimes also analyzed by ImageJ software (https://imagej.nih.gov/ij/).

Real-Time quantitative PCR (qPCR)

Total RNA was isolated from approximately 10 million LCLs (both LCL#1 and LCL#89) either left untreated (DMSO control) or treated with 1 μM MG132 for 12 h using TRIzol reagent according to the manufacturer's instructions (Invitrogen, Thermo Fisher Scientific Inc., Waltham, MA, USA), followed by cDNA preparation using iScript cDNA synthesis kit (BIO-RAD, Hercules, CA, USA) as per manufacturer's protocol. RNA and cDNA quality and quantity were checked using Synergy H1 Multimode Microplate Reader (BioTek Instruments, Inc., VT, USA). qPCR analysis was performed using iTaq Universal SYBR Green Supermix (BIO-RAD, Hercules, CA, USA) in CFX Connect Real-Time PCR detection System (BIO-RAD, Hercules, CA, USA) with the following thermal profile– 1 cycle: 95˚C for 10 min; 40 cycles: 95˚C for 15 sec followed by 60˚C for 1 min; and finally the dissociation curve at– 95˚C for 1 min, 55˚C 30 min, and 95˚C for 30 sec. Unless and otherwise stated, each sample was performed in duplicate and calculation was made using a $2^{-\Delta\Delta CT}$ method to quantify relative expression compared with housekeeping gene controls–B2M, GAPDH and RPLPO. The real time PCR primers used in this study were designed from Primer-BLAST (https://www.ncbi.nlm.nih.gov/tools/primer-blast/) and listed in S2 Table. Real-time PCR primers were obtained from Integrated DNA Technologies, Inc. (Coralville, IA, USA).

RNA-Sequencing and data analyses

Approximately 1 μg of total RNA isolated from LCLs (both LCL#1 and LCL#89) either left untreated (DMSO control) or treated with 1 μM MG132 for 12 h was subjected to whole transcriptome enrichment through selective depletion of 99.9% of ribosomal RNA using RiboMinus Eukaryote Kit for RNA-Seq (Thermo Fisher Scientific Inc., Waltham, MA, USA) followed by library generation using Ion Total RNA-Seq Kit v2 (Thermo Fisher Scientific Inc., Waltham, MA, USA). Transcriptome analysis was performed in Ion S5 XL System (Thermo Fisher Scientific Inc., Waltham, MA, USA). Reads generated from Ion S5 XL were subjected to further analysis with a minimum read length of 25 bp. The filtered in reads were aligned to human genome (hg19) using two-step alignment method. Reads were aligned using STAR and Bowtie software using default parameters. Both Alignment data were merged together using Picard. Reads aligning to reference genome were provided in bam format. Using the encode gene annotations for human genome (hg19), aligned reads were counted for each gene and were represented in standard format for all 4 samples. RNASeqAnalysis plugin (v5.2.0.5) was utilized to perform the analysis and produce gene counts for all the samples.

Using DESeq2 package from R, study for differential expression analysis was performed between sample conditions. It followed the negative binomial distribution for studying gene counts and tested each gene from samples for expression. Genes were selected based on p-value as $< = 0.05$ and $\log_2$ Fold Change as 2 and above (up-regulated) and -2 and below (down-regulated). Differentially expressed gene sets were segregate together and subsequently uploaded on DAVID (Database for Annotation, Visualization and Integrated Discovery, version 6.8) webserver (https://david.ncifcrf.gov/) for further analyses. Features observed in different databases are clustered together for functional analysis. Gene Ontology (GO) was selected from the hits table for DAVID clustering. The clusters were represented through statistical analysis providing P-value and FDR (false discovery rate) in order to select functional significant clusters.

Induction of EBV lytic cycle from LCLs

~10 x 10^6 LCLs (both LCL#1 and LCL#89) were induced to release virus in complete RPMI 1640 medium containing 20 ng/ml TPA (Sigma-Aldrich Corp. St. Louis, MO, USA) and 3 mM sodium butyrate (Sigma-Aldrich Corp. St. Louis, MO, USA) for 24 h. To understand the role of proteasomal inhibition in EBV lytic cycle induction, LCLs were either left untreated (DMSO control) or treated with 1 μM MG132 or bortezomib for 24 h. Cells were then harvested and subjected for genomic DNA isolation using "Blood & Cell Culture DNA Mini Kit" (Qiagen, Hilden, Germany). Reactivation of LCLs was determined by real-time quantitative PCR (qPCR) analyses of EBV DNA targeting *Bam*HI W genomic portion (Forward primer: 5'- CCCAACACTCCACCACA CC-3'; reverse primer: 5'- TCTTAGGAGCTGTCCGAGGG-3'). As described above, the primers were synthesized from Integrated DNA technologies, Inc. (Iowa, USA).

Generation of Beclin 1 and p62 knockdown in HEK293 cells

For Beclin 1 knockdown, approximately 10 x 10^6 HEK293 cells were transfected with pTripZ vector containing sh-Beclin1 (Clone ID: V2THS_23692; GE Healthcare Dharmacon Inc. Lafayette, CO, USA) and sh-p62 sequences under doxycycline inducible promoter by electroporation. For p62 knockdown, 5'-CCTCTGGGCATTGAAGTTGAT-3' sequence was cloned as double stranded oligos using *Xho*I/*Mlu*I restriction sites in pTripZ vector. Sh-RNA expression was initiated using 1 μg/ml doxycycline (Sigma-Aldrich Corp. St. Louis, MO, USA) and transfected cells were selected using 2 μg/ml of puromycin (Sigma-Aldrich Corp. St. Louis, MO, USA) for 7 days. For both cell lines without doxycycline treatment was served as control.

Lentivirus mediated knockdown of EBNA3C in LCLs

For EBNA3C knockdown in LCLs, ~10 x 10^6 HEK293T cells (70% confluency) were first transfected with lentiviral packaging vectors pCMV-VSV-G, pRSV-Rev and pMDLg/pRRE along with pGipZ vector either expressing control sh-RNA (5′-TCTCGCTTGGGCGAGAG TAAG-3′) or sh-EBNA3C (5'-CCATATACCGCAAGGAAT-3'). Lentivirus production and transduction LCLs were essentially carried out as previously described. 12 h post-transfection, the medium was changed with fresh DMEM supplemented with 10 mM sodium butyrate for virus induction for 8 h. Lentivirus was collected twice per day (every 10–12 h) for 2 days in RPMI 1640 supplemented with 10% FBS and 10 mM HEPES, filtered through 0.45 μM filters (Corning Inc., NY, USA) to avoid any cell contamination. The supernatant containing virus was concentrated (100x) by ultra-centrifugation at 70,000 × g for 2.5 h and subsequently used for infection in the presence of 10 μg/ml Polybrene solution (Sigma-Aldrich Corp. St. Louis, MO, USA). 3-days post-infection cells were selected using 1 μg/ml puromycin for 14 days. Selected cells were grown in complete RPMI supplemented with 1 μg/ml puromycin for 1 month before subjected to western blot and cell viability analyses.

Colony formation assays

~10 x 10^6 HEK293 stably transfected with pTripz-Sh-Beclin1 were either left untreated or treated with doxycycline to express the sh-RNA. 72 h post-treatment approximately 1 x 10^6 cells were further treated with DMSO control or 20 μM MG132 for 4 h in 100 mm petri-plates and selected in complete DMEM supplemented with 2 μg/ml puromycin. Two weeks later, cells were fixed with 4% paraformaldehyde paraformaldehyde (Sigma-Aldrich Corp. St. Louis, MO) at room temperature for 0.5 h and stained with 0.1% crystal violet solution (Sigma-Aldrich Corp. St. Louis, MO, USA) for 0.5 h. The plates were scanned using Odyssey CLx Imaging System (LiCor Inc., Lincoln, NE, USA) and the relative colony number was measured by Image J software.

Co-immunoprecipitation assay

~15 x 10^6 HEK293 cells transiently transfected with the indicated expression plasmids or 20 million LCLs were harvested, washed twice with ice cold 1 x PBS and subsequently lysed with 0.5 ml ice cold RIPA buffer, supplemented with protease inhibitors for 1 h on ice with brief vortexing every 5–10 minutes. The lysates were centrifuged at 13,000 rpm for 15 min at 4˚C. 5 μl of each sample was taken out separately for measuring protein concentration using Bradford protein assay reagent (BIO-RAD, Hercules, CA, USA). 5% of the lysates were boiled with 2 x laemmli buffer (BIO-RAD, Hercules, CA, USA) and used as input. Lysates were precleared with control antibody plus 30 μL of 1:1 Protein-A/G magnetic beads (BIO-RAD, Hercules, CA, USA) for 1 h at 4˚C. The protein of interest was captured by rotating the remaining lysate with 1 μg of specific antibody overnight at 4˚C. Immuno-complexes were captured with 30 μL magnetic Protein-A/G beads, pelleted and washed 5 x with ice cold RIPA buffer. Input lysates and IP complexes were boiled in 2 x laemmli buffer, fractionated by SDS-PAGE and transferred to either 0.45 μm nitrocellulose or PVDF membrane for western blot analyses as described above on an Odyssey imager.

In vivo ubiquitination assay

~15 x 10^6 HEK293 cells were transfected with flag-tagged EBNA3C constructs expressing either full-length protein (residues 1–992) or various domains N-terminal (residues 1–365), middle part (residues 366–620) and the C-terminal (residues 621–992). 36 h post-transfection cells were further incubated with 20 μM MG132 for an additional 4 h before harvesting. After washing with 1 x PBS, cells were lysed in 100 μl RIPA buffer containing 1% SDS, boiled for 10 minutes to disrupt any protein-protein interaction. Each lysate was subsequently mixed with 900 μl of RIPA buffer without SDS to dilute the SDS concentration to 0.1%, incubated at 4˚C on rotator for 1 h and centrifuged at 13,000 rpm for 15 min at 4˚C. The supernatant was collected to a new tube and precleared with control antibody plus 30 μL of 1:1 Protein-A/G magnetic beads for 1 h at 4˚C. Flag-tagged EBNA3C proteins were immunoprecipitated with 2 μg M2 antibody for overnight at 4˚C, captured by 1:1 Protein-A/G magnetic beads, washed 5 x with ice cold RIPA buffer, and boiled in 2 x laemmli buffer. The extent of ubiquitination of flag-tagged proteins was determined by SDS-PAGE followed by western blot analysis using indicated antibodies against total ubiquitin or specific to K48- or K63-linked polyubiquitination.

Subcellular fractionation assay

~10 x 10^6 HEK293 cells transiently transfected for 36 h with the indicated EBNA3C expression plasmids were either left untreated (DMSO control) or treated with 20 μM MG132. Cells were harvested and subsequently subjected to subcellular fractionation as per manufacturer's protocol (BIO-RAD, Hercules, CA, USA). Nuclear and cytoplasmic protein fractions were measured by Bradford protein assay (BIO-RAD, Hercules, CA) and ~50 μg of total protein was resolved by SDS-PAGE. The efficiency of nuclear and cytoplasmic fractionation was confirmed by western blot analyses against nuclear protein Histone or lamin A/C and cytoplasmic protein GAPDH, respectively.

Soft agar assay

Soft agar assays were performed for B-cells—LCL#1, LCL#89, BJAB cells stably transfected either vector control or EBNA3C expression construct. 0.75% agar (Sigma-Aldrich Corp. St. Louis, MO, USA) in 1 ml complete RPMI 1640 medium was poured into each well of 6-well

plates (Corning Inc., NY, USA) and set aside to solidify. Next, 1×10^5 LCLs either left untreated (DMSO control) or treated with MG132 (1–5 μM) or bortezomib (0.5–1 μM) for 24 h, were harvested, mixed with 1 ml complete RPMI 1640 medium supplemented with 0.36% agar and poured on the top of the hard agar (1%) layer. Two weeks later, colonies were stained with 0.1% crystal violet for 30 minutes and scanned using Odyssey CLx Imaging System (LiCor Inc., Lincoln, NE, USA) and the relative colony number was measured by Image J software. Prior to staining, each well was also photographed (bright-field) using a ZOE Fluorescent Cell Imager (BIO-RAD, Hercules, CA, USA).

Cell viability assay

~0.5×10^5 cells plated into each well of the six-well plates (Corning Inc., NY, USA) were treated with either MG132 or bortezomib at increasing concentrations (0–10 μM) for the indicated time points at 37˚C in a humidified CO_2 chamber. Viable cells from each well were measured by Trypan blue exclusion method using an automated cell counter (BIO-RAD, Hercules, CA). Experiments were performed in duplicate and were independently repeated two times.

Apoptosis assay

Cell apoptosis induced by proteasomal inhibitors was determined by Annexin V-FITC Apoptosis Staining / Detection Kit (ab14085) according to manufacturer's protocol (Abcam Cambridge, UK). ~5 x 10^5 BJAB cells stably harboring empty vector (BJAB-vector) or EBNA3C expression construct (BJAB-EBNA3C) along with lymphoblastoid cell lines (both LCL1 and LCL89) were either left untreated (DMSO control) or treated with proteasomal inhibitors—MG132 and bortezomib for 24 h. Post treatment cells were collected by centrifugation and re-suspended in 500 μL of 1X binding buffer. Next, cells were stained with 5 μL of annexin V-FITC and 5 μL of propidium iodide (Sigma-Aldrich Corp. St. Louis, MO, USA) for 5 min at room temperature in the dark. FITC labeled annexin V binding (Ex = 488 nm; Em = 350 nm) and PI staining were detected using FITC signal detector by the phycoerythrin emission signal detector in BD FACSAria III (BD Biosciences, San Jose, CA, USA). Experiments were performed in duplicate and presented the data as an average with SE+/-.

Measurement of intracellular ROS

~1×10^5 LCLs (both LCL#1 and LCL#89) either left untreated (DMSO control) or treated with 0.5 μM MG132 in the presence and absence of ROS (Reactive Oxygen Species) scavenger 1 mM N-Acetyl-L-cysteine (NAC) for 24 h were harvested, suspended in PBS in a 96-well plate (Corning Inc., NY, USA). The fluorescent probe DCFH-DA (Sigma-Aldrich Corp. St. Louis, MO, USA) was used to detect intracellular ROS levels. After incubation with 20μM DCFH-DA for 30 min at 37˚C and the fluorescence was measured by Synergy H1 Multimode Microplate Reader (BioTek Instruments, Inc., VT, USA) using the blue filter (485 nm) for excitation and the green filter (528 nm) for emission. Experiments were performed in triplicate and were independently repeated two times.

Statistical analysis

All the data represented are as the mean values with standard deviation (SD). Statistical significance of differences in the mean values was analyzed using the Student's t-test two tail distribution and equal variances between two samples. P-value below 0.05 was considered as significant ($^*P < 0.05$; $^{**}P < 0.01$; $^{***}P < 0.001$; ns, not significant).

Supporting information

S1 Fig. Effect of proteasomal and lysosomal inhibitors on EBV latent antigens. ~10 x 10^6 (A) BJAB stably expressing EBNA3A (BJAB#E3A), (B) BJAB stably expressing EBNA3C (BJAB#E3C), (C) LCL#1, (D) LCL#89 cells either left untreated (DMSO control) or treated with (A-D) 1 μM MG132, (C) 50 μM chloroquine, CQ (D) 0.5 μM bortezomib for 12 h, were harvested and subjected for western blot analyses using the indicated antibodies. GAPDH blot was used as loading control. Protein bands were quantified by Odyssey imager software and indicated as bar diagrams at the bottom of corresponding lanes.
(TIF)

S2 Fig. Proteasomal inhibition leads to transcriptional activation of both viral and autophagy genes in LCLs. (A-D) ~10 x 10^6 two LCL clones–LCL#1 and LCL#89 either left untreated (DMSO control) or treated with 0.5 μM bortezomib. 12 h post-treatment cells were harvested for (A and C) total RNA or (B and D) genomic DNA isolation as described in Fig 3. (B and D) LCLs were treated with 3 mM sodium butyrate (NaBu) in combination with 20 ng/ml 12-O-tetradecanoylphorbol-13-acetate (TPA) for 24 h to induce viral lytic cycle as positive control. (A and C) Total RNA was subjected to cDNA preparation followed by qPCR analyses for the selected viral genes. (B and D) qPCR was performed for the detection of EBV DNA (BamHW fragment) using the genomic DNA isolated from each sample. The average fold increase of two independent experiments represented as bar diagrams was calculated in comparison to DMSO control using the $2^{-\Delta\Delta Ct}$ method taking GAPDH as genomic control. (E-F) qPCR analyses of the selected cellular genes as described in (A and C). (G-H) BJAB cells stably expressing (G) EBNA3A (BJAB#E3A) or (H) EBNA3C (BJAB#E3C) either left untreated (DMSO control) or treated with 1 μM MG132 for 12 h were harvested. Total RNA was subjected to cDNA preparation followed by qPCR analyses for the selected viral and cellular gene expressions. (A, C, E-H) For all qPCR analyses, the relative changes in transcripts (log10) using the $2^{-\Delta\Delta Ct}$ method are represented as bar diagrams in comparison to DMSO control using GAPDH and B2M as housekeeping genes. Two independent experiments were carried out in similar settings and results represent as an average value for each transcript. Average values +/- SEM are plotted. *, **, *** = p-value < 0.01, 0.005 and 0.001 respectively.
(TIF)

S3 Fig. Proteasomal inhibition does not affect splicing pattern of EBNA3 genes. (A) The gene structure of the EBNA3 family (EBNA3A, EBNA3B and EBNA3C) is illustrated, and the names and positions of primers are indicated. Introns and exons are indicated in red and black, respectively. The diagram is not drawn to scale. While primers set 1 indicated as red amplifies intronic region, primers set 2 indicated as green amplifies exclusively exonic region. (B-C) ~10 x 10^6 two LCL clones–LCL#1 and LCL#89 either left untreated (DMSO control) or treated with 1 μM MG132 for 12 h were harvested for total RNA isolation and subjected to cDNA preparation followed by qPCR analyses for EBNA3 family genes using both primer sets. (B) The relative changes in transcripts (log10) using the $2^{-\Delta\Delta Ct}$ method are represented as bar diagrams in comparison to DMSO control using GAPDH and B2M as housekeeping genes. Two independent experiments were carried out in similar settings and results represent as an average value for each transcript. Average values +/- SEM are plotted. *** = p-value < 0.001 respectively. (C) Agarose gel electrophoresis of end product of each PCR reaction.
(TIF)

S4 Fig. Effect of p62 knockdown on EBNA3C degradation in response to proteasomal inhibition. (A) HEK293 cells stably transfected with pTripz-mCherry-Sh-p62 construct expressing sh-p62 under doxycycline (Dox) inducible promoter was treated with 1 μg/ml doxycycline for

48 h and photographed using a fluorescent cell imager. Scale bars, 100 μm. (B-C) 48 h post-treatment, efficiency of p62 knockdown was tested using (B) qRT-PCR and (C) western blot analyses. For qRT-PCR analyses, the relative changes in transcripts using the $2^{-\Delta\Delta Ct}$ method are represented as bar diagrams in comparison to no DOX control using B2M as housekeeping gene. (D) Cells were further transfected either empty vector (pA3M) or myc-tagged EBNA3C expressing construct. 36 h post-transfection cells were either left untreated or treated with 20 μM MG132. 4 h post-treatment cells were harvested, washed with 1 x PBS, lysed in RIPA buffer and subjected for western blot analyses for the indicated antibodies. For western blot analyses, GAPDH blot was used as loading control. Protein bands were quantified by Odyssey imager software and represented as bar diagrams at the bottom of corresponding lanes.
(TIF)

S5 Fig. High exposure of Fig 7A and 7D. For **a** better view of protein bands in Fig 7A and 7D, intensities are increased (~3 fold) using Odyssey imager software.
(TIF)

S6 Fig. EBNA3C fractionation in the absence and presence of leptomycin B. HEK293 cells transiently transfected with flag-tagged EBNA3C construct either left untreated (DMSO control) or treated with leptomycin B (LMB; 20 ng/ml) for 24 h, were subjected to subcellular fractionation as described in the "Materials and Methods" section. Protein bands were quantified by Odyssey imager software and indicated as bar diagrams at the bottom of corresponding lanes.
(TIF)

S7 Fig. The N-terminal domain of EBNA3C plays crucial role in forming complex with p62 and LC3B. (A) HEK293 cells transiently transfected with expression plasmids for flag-tagged EBNA3C truncations (residues 1–365, 366–621 and 621–992) were subjected to co-immunoprecipitation study with anti-flag antibody. Western blots were performed with the indicated antibodies by stripping and reprobing the same membrane. * indicates IgG bands. (B) Schematic representation of EBNA3C truncations used in the co-immunoprecipitation experiment. (C-D) Summary and cartoon representation of the interaction study of different EBNA3C domains with p62 and LC3B.
(TIF)

S8 Fig. Caspase inhibitor does not rescue MG132-induced EBNA3C's degradation. LCLs were either left untreated (DMSO control) or treated with 1 μM MG132, 50 μM pan-caspase inhibitor Z-VAD(OMe)-FMK (Z-VAD) or MG132 plus Z-VAD. 24 h post-treatment cells were subjected for either (A) western blot analysis or (B) immunostaining with the indicated antibodies. Each panel in (B) is representative picture of two independent experiments and nuclei were counterstained by DAPI before mounting the cells. Scale bars, 5 μm. In (A) GAPDH blot was used as loading control and protein bands were quantified by Odyssey imager software and represented as bar diagrams at the bottom of corresponding lanes.
(TIF)

S9 Fig. MG132 mediated ROS generation has no role in EBNA3C degradation. LCLs were either left untreated (DMSO control) or treated with 0.5 μM MG132, 1 mM N-Acetyl-L-cysteine (NAC) or MG132 plus NAC. 24 h post-treatment, cells were subjected for (A-B) ROS (Reactive Oxygen Species) measurement using DCFH-DA fluorescent probe, (C) western blot analysis and (D) immunostaining with the indicated antibodies. (C) GAPDH blot was used as loading control and protein bands were quantified by Odyssey imager software and represented as bar diagrams at the bottom of corresponding lanes. Each panel in (D) corresponds to

single experiment of two independent experiments and nuclei were counterstained by DAPI before mounting the cells. Scale bars, 5 μm.
(TIF)

S10 Fig. Effect of proteasomal and lysosomal inhibitors on EBV positive and negative B-cell lymphoma cells. ~10 x 10^6 cells were harvested, lysed in RIPA buffer and subjected to western blot analyses with anti-GAPDH (as loading control) and anti-EBNA3C antibodies.
(TIF)

S11 Fig. EBNA3C expressing cells are sensitive towards proteasome inhibitors but not to autophagy inhibitors. ~10 x 10^6 cells were harvested, lysed in RIPA buffer and subjected to western blot analyses with anti-GAPDH (as loading control) and anti-EBNA3C antibodies.
(TIF)

S1 Table. RNA-Seq and Gene Ontology term analyses of DMSO and MG132 treated LCLs. ~10 x 10^6 LCL#1 and LCL#89 either left untreated or treated with 1 μM MG132 for 12 h, were subjected to RNA-Seq followed by Gene Ontology (GO)-Term Enrichment analyses as described in the "Materials and Methods" section.
(XLSX)

S2 Table. Real-time PCR primers. Real-time PCR primers for both viral and cellular genes were designed from Primer-BLAST (https://www.ncbi.nlm.nih.gov/tools/primer-blast/). Reference Sequence ID (RefSeq ID) of each gene is mentioned. All primers were selected at annealing temperature of ~60˚C. RefSeq ID of each gene is mentioned.
(DOCX)

Acknowledgments

We sincerely thank to Elliott Kieff (Harvard Medical School, USA), Martin Rowe (University of Birmingham, UK), Jayanta Debnath (University of California, San Francisco, USA), Edward M. Campbell (Loyola University Chicago, USA), Robert A. Weinberg (Whitehead Institute for Biomedical research, Cambridge, USA), Rupak Dutta (Indian Institute of Science Education and Research, Kolkata, India), Nabendu Biswas (Presidency University, Kolkata, India) and National Centre for Cell Science (NCCS), Dept. of Biotechnology (DBT), Govt. of India for providing reagents, plasmids, cell lines and hybridomas. We thank Rupak Dutta (Indian Institute of Science Education and Research, Kolkata, India) and Shubhra Majumder (Presidency University, Kolkata, India) for careful review of the manuscript. We also thank Pralay Majumder (Presidency University, Kolkata, India) for technical support in using Microscopy Facility at Dept. Life Sciences, Presidency University, Kolkata, India.

Author Contributions

Conceptualization: Abhik Saha.

Data curation: Chandrima Gain, Samaresh Malik, Shaoni Bhattacharjee, Arijit Ghosh, Abhik Saha.

Formal analysis: Chandrima Gain, Samaresh Malik, Shaoni Bhattacharjee, Arijit Ghosh, Benu Brata Das, Abhik Saha.

Funding acquisition: Abhik Saha.

Investigation: Chandrima Gain, Shaoni Bhattacharjee, Abhik Saha.

Methodology: Chandrima Gain, Samaresh Malik, Shaoni Bhattacharjee, Arijit Ghosh, Benu Brata Das, Abhik Saha.

Project administration: Abhik Saha.

Resources: Erle S. Robertson, Benu Brata Das, Abhik Saha.

Software: Erle S. Robertson, Abhik Saha.

Supervision: Abhik Saha.

Validation: Chandrima Gain, Samaresh Malik, Abhik Saha.

Visualization: Chandrima Gain, Abhik Saha.

Writing – original draft: Chandrima Gain, Abhik Saha.

Writing – review & editing: Abhik Saha.

References

1. Saha A, Robertson ES (2011) Epstein-Barr virus-associated B-cell lymphomas: pathogenesis and clinical outcomes. Clin Cancer Res 17: 3056–3063. https://doi.org/10.1158/1078-0432.CCR-10-2578 PMID: 21372216
2. Saha A, Robertson ES (2019) Mechanisms of B-Cell Oncogenesis Induced by Epstein-Barr Virus. J Virol 93.
3. Young LS, Yap LF, Murray PG (2016) Epstein-Barr virus: more than 50 years old and still providing surprises. Nat Rev Cancer 16: 789–802. https://doi.org/10.1038/nrc.2016.92 PMID: 27687982
4. Shannon-Lowe C, Rickinson AB, Bell AI (2017) Epstein-Barr virus-associated lymphomas. Philos Trans R Soc Lond B Biol Sci 372.
5. Vetsika EK, Callan M (2004) Infectious mononucleosis and Epstein-Barr virus. Expert Rev Mol Med 6: 1–16.
6. McFadden K, Hafez AY, Kishton R, Messinger JE, Nikitin PA, et al. (2016) Metabolic stress is a barrier to Epstein-Barr virus-mediated B-cell immortalization. Proc Natl Acad Sci U S A 113: E782–790. https://doi.org/10.1073/pnas.1517141113 PMID: 26802124
7. Hussain T, Mulherkar R (2012) Lymphoblastoid Cell lines: a Continuous in Vitro Source of Cells to Study Carcinogen Sensitivity and DNA Repair. Int J Mol Cell Med 1: 75–87. PMID: 24551762
8. Maruo S, Wu Y, Ishikawa S, Kanda T, Iwakiri D, et al. (2006) Epstein-Barr virus nuclear protein EBNA3C is required for cell cycle progression and growth maintenance of lymphoblastoid cells. Proc Natl Acad Sci U S A 103: 19500–19505. https://doi.org/10.1073/pnas.0604919104 PMID: 17159137
9. Tomkinson B, Robertson E, Kieff E (1993) Epstein-Barr virus nuclear proteins EBNA-3A and EBNA-3C are essential for B-lymphocyte growth transformation. J Virol 67: 2014–2025. PMID: 8445720
10. Szymula A, Palermo RD, Bayoumy A, Groves IJ, Ba Abdullah M, et al. (2018) Epstein-Barr virus nuclear antigen EBNA-LP is essential for transforming naive B cells, and facilitates recruitment of transcription factors to the viral genome. PLoS Pathog 14: e1006890. https://doi.org/10.1371/journal.ppat.1006890 PMID: 29462212
11. Dirmeier U, Neuhierl B, Kilger E, Reisbach G, Sandberg ML, et al. (2003) Latent membrane protein 1 is critical for efficient growth transformation of human B cells by epstein-barr virus. Cancer Res 63: 2982–2989. PMID: 12782607
12. Cohen JI, Wang F, Mannick J, Kieff E (1989) Epstein-Barr virus nuclear protein 2 is a key determinant of lymphocyte transformation. Proc Natl Acad Sci U S A 86: 9558–9562. https://doi.org/10.1073/pnas.86.23.9558 PMID: 2556717
13. Allday MJ, Bazot Q, White RE (2015) The EBNA3 Family: Two Oncoproteins and a Tumour Suppressor that Are Central to the Biology of EBV in B Cells. Curr Top Microbiol Immunol 391: 61–117. https://doi.org/10.1007/978-3-319-22834-1_3 PMID: 26428372
14. Bhattacharjee S, Ghosh Roy S, Bose P, Saha A (2016) Role of EBNA-3 Family Proteins in EBV Associated B-cell Lymphomagenesis. Front Microbiol 7: 457. https://doi.org/10.3389/fmicb.2016.00457 PMID: 27092119
15. Saha A, Robertson ES (2013) Impact of EBV essential nuclear protein EBNA-3C on B-cell proliferation and apoptosis. Future Microbiol 8: 323–352. https://doi.org/10.2217/fmb.12.147 PMID: 23464371

16. Yenamandra SP, Sompallae R, Klein G, Kashuba E (2009) Comparative analysis of the Epstein-Barr virus encoded nuclear proteins of EBNA-3 family. Comput Biol Med 39: 1036–1042. https://doi.org/10.1016/j.compbiomed.2009.08.006 PMID: 19762010

17. Lilienbaum A (2013) Relationship between the proteasomal system and autophagy. Int J Biochem Mol Biol 4: 1–26. PMID: 23638318

18. Dikic I (2017) Proteasomal and Autophagic Degradation Systems. Annu Rev Biochem 86: 193–224. https://doi.org/10.1146/annurev-biochem-061516-044908 PMID: 28460188

19. Yeh TC, Bratton SB (2013) Caspase-dependent regulation of the ubiquitin-proteasome system through direct substrate targeting. Proc Natl Acad Sci U S A 110: 14284–14289. https://doi.org/10.1073/pnas.1306179110 PMID: 23940367

20. Laussmann MA, Passante E, Dussmann H, Rauen JA, Wurstle ML, et al. (2011) Proteasome inhibition can induce an autophagy-dependent apical activation of caspase-8. Cell Death Differ 18: 1584–1597. https://doi.org/10.1038/cdd.2011.27 PMID: 21455219

21. Ding WX, Ni HM, Gao W, Yoshimori T, Stolz DB, et al. (2007) Linking of autophagy to ubiquitin-proteasome system is important for the regulation of endoplasmic reticulum stress and cell viability. Am J Pathol 171: 513–524. https://doi.org/10.2353/ajpath.2007.070188 PMID: 17620365

22. Bellot G, Garcia-Medina R, Gounon P, Chiche J, Roux D, et al. (2009) Hypoxia-induced autophagy is mediated through hypoxia-inducible factor induction of BNIP3 and BNIP3L via their BH3 domains. Mol Cell Biol 29: 2570–2581. https://doi.org/10.1128/MCB.00166-09 PMID: 19273585

23. Pankiv S, Clausen TH, Lamark T, Brech A, Bruun JA, et al. (2007) p62/SQSTM1 binds directly to Atg8/LC3 to facilitate degradation of ubiquitinated protein aggregates by autophagy. J Biol Chem 282: 24131–24145. https://doi.org/10.1074/jbc.M702824200 PMID: 17580304

24. Birgisdottir AB, Lamark T, Johansen T (2013) The LIR motif—crucial for selective autophagy. J Cell Sci 126: 3237–3247. https://doi.org/10.1242/jcs.126128 PMID: 23908376

25. Shaid S, Brandts CH, Serve H, Dikic I (2013) Ubiquitination and selective autophagy. Cell Death Differ 20: 21–30. https://doi.org/10.1038/cdd.2012.72 PMID: 22722335

26. Kaur J, Debnath J (2015) Autophagy at the crossroads of catabolism and anabolism. Nat Rev Mol Cell Biol 16: 461–472. https://doi.org/10.1038/nrm4024 PMID: 26177004

27. Knight JS, Sharma N, Robertson ES (2005) Epstein-Barr virus latent antigen 3C can mediate the degradation of the retinoblastoma protein through an SCF cellular ubiquitin ligase. Proc Natl Acad Sci U S A 102: 18562–18566. https://doi.org/10.1073/pnas.0503886102 PMID: 16352731

28. Knight JS, Sharma N, Robertson ES (2005) SCFSkp2 complex targeted by Epstein-Barr virus essential nuclear antigen. Mol Cell Biol 25: 1749–1763. https://doi.org/10.1128/MCB.25.5.1749-1763.2005 PMID: 15713632

29. Saha A, Halder S, Upadhyay SK, Lu J, Kumar P, et al. (2011) Epstein-Barr virus nuclear antigen 3C facilitates G1-S transition by stabilizing and enhancing the function of cyclin D1. PLoS Pathog 7: e1001275. https://doi.org/10.1371/journal.ppat.1001275 PMID: 21347341

30. Saha A, Murakami M, Kumar P, Bajaj B, Sims K, et al. (2009) Epstein-Barr virus nuclear antigen 3C augments Mdm2-mediated p53 ubiquitination and degradation by deubiquitinating Mdm2. J Virol 83: 4652–4669. https://doi.org/10.1128/JVI.02408-08 PMID: 19244339

31. Banerjee S, Lu J, Cai Q, Sun Z, Jha HC, et al. (2014) EBNA3C augments Pim-1 mediated phosphorylation and degradation of p21 to promote B-cell proliferation. PLoS Pathog 10: e1004304. https://doi.org/10.1371/journal.ppat.1004304 PMID: 25121590

32. Bajaj BG, Murakami M, Cai Q, Verma SC, Lan K, et al. (2008) Epstein-Barr virus nuclear antigen 3C interacts with and enhances the stability of the c-Myc oncoprotein. J Virol 82: 4082–4090. https://doi.org/10.1128/JVI.02500-07 PMID: 18256156

33. Touitou R, O'Nions J, Heaney J, Allday MJ (2005) Epstein-Barr virus EBNA3 proteins bind to the C8/alpha7 subunit of the 20S proteasome and are degraded by 20S proteasomes in vitro, but are very stable in latently infected B cells. J Gen Virol 86: 1269–1277. https://doi.org/10.1099/vir.0.80763-0 PMID: 15831937

34. Paludan C, Schmid D, Landthaler M, Vockerodt M, Kube D, et al. (2005) Endogenous MHC class II processing of a viral nuclear antigen after autophagy. Science 307: 593–596. https://doi.org/10.1126/science.1104904 PMID: 15591165

35. Taylor GS, Long HM, Haigh TA, Larsen M, Brooks J, et al. (2006) A role for intercellular antigen transfer in the recognition of EBV-transformed B cell lines by EBV nuclear antigen-specific CD4+ T cells. J Immunol 177: 3746–3756. https://doi.org/10.4049/jimmunol.177.6.3746 PMID: 16951335

36. Bhattacharjee S, Bose P, Patel K, Roy SG, Gain C, et al. (2018) Transcriptional and epigenetic modulation of autophagy promotes EBV oncoprotein EBNA3C induced B-cell survival. Cell Death Dis 9: 605. https://doi.org/10.1038/s41419-018-0668-9 PMID: 29789559

37. Halasi M, Pandit B, Gartel AL (2014) Proteasome inhibitors suppress the protein expression of mutant p53. Cell Cycle 13: 3202–3206. https://doi.org/10.4161/15384101.2014.950132 PMID: 25485499

38. Galindo-Moreno M, Giraldez S, Saez C, Japon MA, Tortolero M, et al. (2017) Both p62/SQSTM1-HDAC6-dependent autophagy and the aggresome pathway mediate CDK1 degradation in human breast cancer. Sci Rep 7: 10078. https://doi.org/10.1038/s41598-017-10506-8 PMID: 28855742

39. Harhouri K, Navarro C, Depetris D, Mattei MG, Nissan X, et al. (2017) MG132-induced progerin clearance is mediated by autophagy activation and splicing regulation. EMBO Mol Med 9: 1294–1313. https://doi.org/10.15252/emmm.201607315 PMID: 28674081

40. Sun L, Shen X, Liu Y, Zhang G, Wei J, et al. (2010) The location of endogenous wild-type p53 protein in 293T and HEK293 cells expressing low-risk HPV-6E6 fusion protein with GFP. Acta Biochim Biophys Sin (Shanghai) 42: 230–235. https://doi.org/10.1093/abbs/gmq009 PMID: 20213049

41. Leung CS, Haigh TA, Mackay LK, Rickinson AB, Taylor GS (2010) Nuclear location of an endogenously expressed antigen, EBNA1, restricts access to macroautophagy and the range of CD4 epitope display. Proc Natl Acad Sci U S A 107: 2165–2170. https://doi.org/10.1073/pnas.0909448107 PMID: 20133861

42. Tellam J, Sherritt M, Thomson S, Tellam R, Moss DJ, et al. (2001) Targeting of EBNA1 for rapid intracellular degradation overrides the inhibitory effects of the Gly-Ala repeat domain and restores CD8+ T cell recognition. J Biol Chem 276: 33353–33360. https://doi.org/10.1074/jbc.M104535200 PMID: 11435434

43. White RE, Groves IJ, Turro E, Yee J, Kremmer E, et al. (2010) Extensive co-operation between the Epstein-Barr virus EBNA3 proteins in the manipulation of host gene expression and epigenetic chromatin modification. PLoS One 5: e13979. https://doi.org/10.1371/journal.pone.0013979 PMID: 21085583

44. Paschos K, Bazot Q, Ho G, Parker GA, Lees J, et al. (2016) Core binding factor (CBF) is required for Epstein-Barr virus EBNA3 proteins to regulate target gene expression. Nucleic Acids Res.

45. White RE, Ramer PC, Naresh KN, Meixlsperger S, Pinaud L, et al. (2012) EBNA3B-deficient EBV promotes B cell lymphomagenesis in humanized mice and is found in human tumors. J Clin Invest 122: 1487–1502. https://doi.org/10.1172/JCI58092 PMID: 22406538

46. Aviel S, Winberg G, Massucci M, Ciechanover A (2000) Degradation of the epstein-barr virus latent membrane protein 1 (LMP1) by the ubiquitin-proteasome pathway. Targeting via ubiquitination of the N-terminal residue. J Biol Chem 275: 23491–23499. https://doi.org/10.1074/jbc.M002052200 PMID: 10807912

47. Lee DY, Sugden B (2008) The latent membrane protein 1 oncogene modifies B-cell physiology by regulating autophagy. Oncogene 27: 2833–2842. https://doi.org/10.1038/sj.onc.1210946 PMID: 18037963

48. Kane RC, Bross PF, Farrell AT, Pazdur R (2003) Velcade: U.S. FDA approval for the treatment of multiple myeloma progressing on prior therapy. Oncologist 8: 508–513. https://doi.org/10.1634/theoncologist.8-6-508 PMID: 14657528

49. Li H, Hu J, Luo X, Bode AM, Dong Z, et al. (2018) Therapies based on targeting Epstein-Barr virus lytic replication for EBV-associated malignancies. Cancer Sci 109: 2101–2108. https://doi.org/10.1111/cas.13634 PMID: 29751367

50. Westphal EM, Blackstock W, Feng W, Israel B, Kenney SC (2000) Activation of lytic Epstein-Barr virus (EBV) infection by radiation and sodium butyrate in vitro and in vivo: a potential method for treating EBV-positive malignancies. Cancer Res 60: 5781–5788. PMID: 11059774

51. Cen H, McKnight JL (1994) EBV-immortalized isogenic human B-cell clones exhibit differences in DNA-protein complex formation on the BZLF1 and BRLF1 promoter regions among latent, lytic and TPA-activated cell lines. Virus Res 31: 89–107. https://doi.org/10.1016/0168-1702(94)90073-6 PMID: 8165871

52. Shirley CM, Chen J, Shamay M, Li H, Zahnow CA, et al. (2011) Bortezomib induction of C/EBPbeta mediates Epstein-Barr virus lytic activation in Burkitt lymphoma. Blood 117: 6297–6303. https://doi.org/10.1182/blood-2011-01-332379 PMID: 21447826

53. Kienzle N, Sculley TB, Poulsen L, Buck M, Cross S, et al. (1998) Identification of a cytotoxic T-lymphocyte response to the novel BARF0 protein of Epstein-Barr virus: a critical role for antigen expression. J Virol 72: 6614–6620. PMID: 9658107

54. Xu P, Duong DM, Seyfried NT, Cheng D, Xie Y, et al. (2009) Quantitative proteomics reveals the function of unconventional ubiquitin chains in proteasomal degradation. Cell 137: 133–145. https://doi.org/10.1016/j.cell.2009.01.041 PMID: 19345192

55. Seibenhener ML, Babu JR, Geetha T, Wong HC, Krishna NR, et al. (2004) Sequestosome 1/p62 is a polyubiquitin chain binding protein involved in ubiquitin proteasome degradation. Mol Cell Biol 24: 8055–8068. https://doi.org/10.1128/MCB.24.18.8055-8068.2004 PMID: 15340068

56. Cabe M, Rademacher DJ, Karlsson AB, Cherukuri S, Bakowska JC (2018) PB1 and UBA domains of p62 are essential for aggresome-like induced structure formation. Biochem Biophys Res Commun 503: 2306–2311. https://doi.org/10.1016/j.bbrc.2018.06.153 PMID: 29966650

57. la Cour T, Kiemer L, Molgaard A, Gupta R, Skriver K, et al. (2004) Analysis and prediction of leucine-rich nuclear export signals. Protein Eng Des Sel 17: 527–536. https://doi.org/10.1093/protein/gzh062 PMID: 15314210

58. Jang BC, Munoz-Najar U, Paik JH, Claffey K, Yoshida M, et al. (2003) Leptomycin B, an inhibitor of the nuclear export receptor CRM1, inhibits COX-2 expression. J Biol Chem 278: 2773–2776. https://doi.org/10.1074/jbc.C200620200 PMID: 12468543

59. Park S, Park JA, Yoo H, Park HB, Lee Y (2017) Proteasome inhibitor-induced cleavage of HSP90 is mediated by ROS generation and caspase 10-activation in human leukemic cells. Redox Biol 13: 470–476. https://doi.org/10.1016/j.redox.2017.07.010 PMID: 28715732

60. Halasi M, Wang M, Chavan TS, Gaponenko V, Hay N, et al. (2013) ROS inhibitor N-acetyl-L-cysteine antagonizes the activity of proteasome inhibitors. Biochem J 454: 201–208. https://doi.org/10.1042/BJ20130282 PMID: 23772801

61. McConkey DJ, Zhu K (2008) Mechanisms of proteasome inhibitor action and resistance in cancer. Drug Resist Updat 11: 164–179. https://doi.org/10.1016/j.drup.2008.08.002 PMID: 18818117

62. Crawford LJ, Walker B, Irvine AE (2011) Proteasome inhibitors in cancer therapy. J Cell Commun Signal 5: 101–110. https://doi.org/10.1007/s12079-011-0121-7 PMID: 21484190

63. Bard JAM, Goodall EA, Greene ER, Jonsson E, Dong KC, et al. (2018) Structure and Function of the 26S Proteasome. Annu Rev Biochem 87: 697–724. https://doi.org/10.1146/annurev-biochem-062917-011931 PMID: 29652515

64. Rule S (2018) Bortezomib-based chemotherapy in mantle cell lymphoma. Lancet Oncol 19: 1419–1421. https://doi.org/10.1016/S1470-2045(18)30743-5 PMID: 30348536

65. Kim H, Bhattacharya A, Qi L (2015) Endoplasmic reticulum quality control in cancer: Friend or foe. Semin Cancer Biol 33: 25–33. https://doi.org/10.1016/j.semcancer.2015.02.003 PMID: 25794824

66. Thibaudeau TA, Smith DM (2019) A Practical Review of Proteasome Pharmacology. Pharmacol Rev 71: 170–197. https://doi.org/10.1124/pr.117.015370 PMID: 30867233

67. Ogata M, Hino S, Saito A, Morikawa K, Kondo S, et al. (2006) Autophagy is activated for cell survival after endoplasmic reticulum stress. Mol Cell Biol 26: 9220–9231. https://doi.org/10.1128/MCB.01453-06 PMID: 17030611

68. Rashid HO, Yadav RK, Kim HR, Chae HJ (2015) ER stress: Autophagy induction, inhibition and selection. Autophagy 11: 1956–1977. https://doi.org/10.1080/15548627.2015.1091141 PMID: 26389781

69. Wang D, Xu Q, Yuan Q, Jia M, Niu H, et al. (2019) Proteasome inhibition boosts autophagic degradation of ubiquitinated-AGR2 and enhances the antitumor efficiency of bevacizumab. Oncogene 38: 3458–3474. https://doi.org/10.1038/s41388-019-0675-z PMID: 30647455

70. Goussetis DJ, Gounaris E, Wu EJ, Vakana E, Sharma B, et al. (2012) Autophagic degradation of the BCR-ABL oncoprotein and generation of antileukemic responses by arsenic trioxide. Blood 120: 3555–3562. https://doi.org/10.1182/blood-2012-01-402578 PMID: 22898604

71. Isakson P, Bjoras M, Boe SO, Simonsen A (2010) Autophagy contributes to therapy-induced degradation of the PML/RARA oncoprotein. Blood 116: 2324–2331. https://doi.org/10.1182/blood-2010-01-261040 PMID: 20574048

72. Sariyer IK, Merabova N, Patel PK, Knezevic T, Rosati A, et al. (2012) Bag3-induced autophagy is associated with degradation of JCV oncoprotein, T-Ag. PLoS One 7: e45000. https://doi.org/10.1371/journal.pone.0045000 PMID: 22984599

73. Fang Y, Wang J, Xu L, Cao Y, Xu F, et al. (2016) Autophagy maintains ubiquitination-proteasomal degradation of Sirt3 to limit oxidative stress in K562 leukemia cells. Oncotarget 7: 35692–35702. https://doi.org/10.18632/oncotarget.9592 PMID: 27232755

74. Saha A, Lu J, Morizur L, Upadhyay SK, Aj MP, et al. (2012) E2F1 mediated apoptosis induced by the DNA damage response is blocked by EBV nuclear antigen 3C in lymphoblastoid cells. PLoS Pathog 8: e1002573. https://doi.org/10.1371/journal.ppat.1002573 PMID: 22438805

75. Pei Y, Banerjee S, Sun Z, Jha HC, Saha A, et al. (2016) EBV Nuclear Antigen 3C Mediates Regulation of E2F6 to Inhibit E2F1 Transcription and Promote Cell Proliferation. PLoS Pathog 12: e1005844. https://doi.org/10.1371/journal.ppat.1005844 PMID: 27548379

76. Cai Q, Guo Y, Xiao B, Banerjee S, Saha A, et al. (2011) Epstein-Barr virus nuclear antigen 3C stabilizes Gemin3 to block p53-mediated apoptosis. PLoS Pathog 7: e1002418. https://doi.org/10.1371/journal.ppat.1002418 PMID: 22174681

77. Jacomin AC, Samavedam S, Promponas V, Nezis IP (2016) iLIR database: A web resource for LIR motif-containing proteins in eukaryotes. Autophagy 12: 1945–1953. https://doi.org/10.1080/15548627.2016.1207016 PMID: 27484196

78. Saha A, Bamidele A, Murakami M, Robertson ES (2011) EBNA3C attenuates the function of p53 through interaction with inhibitor of growth family proteins 4 and 5. J Virol 85: 2079–2088. https://doi.org/10.1128/JVI.02279-10 PMID: 21177815

79. Banerjee S, Lu J, Cai Q, Saha A, Jha HC, et al. (2013) The EBV Latent Antigen 3C Inhibits Apoptosis through Targeted Regulation of Interferon Regulatory Factors 4 and 8. PLoS Pathog 9: e1003314. https://doi.org/10.1371/journal.ppat.1003314 PMID: 23658517

80. Yi F, Saha A, Murakami M, Kumar P, Knight JS, et al. (2009) Epstein-Barr virus nuclear antigen 3C targets p53 and modulates its transcriptional and apoptotic activities. Virology 388: 236–247. https://doi.org/10.1016/j.virol.2009.03.027 PMID: 19394062

81. Maruo S, Wu Y, Ito T, Kanda T, Kieff ED, et al. (2009) Epstein-Barr virus nuclear protein EBNA3C residues critical for maintaining lymphoblastoid cell growth. Proc Natl Acad Sci U S A 106: 4419–4424. https://doi.org/10.1073/pnas.0813134106 PMID: 19237563

82. Park YE, Hayashi YK, Bonne G, Arimura T, Noguchi S, et al. (2009) Autophagic degradation of nuclear components in mammalian cells. Autophagy 5: 795–804. https://doi.org/10.4161/auto.8901 PMID: 19550147

83. Dou Z, Xu C, Donahue G, Shimi T, Pan JA, et al. (2015) Autophagy mediates degradation of nuclear lamina. Nature 527: 105–109. https://doi.org/10.1038/nature15548 PMID: 26524528

84. Joseph TW, Zaika A, Moll UM (2003) Nuclear and cytoplasmic degradation of endogenous p53 and HDM2 occurs during down-regulation of the p53 response after multiple types of DNA damage. FASEB J 17: 1622–1630. https://doi.org/10.1096/fj.02-0931com PMID: 12958168

85. Chatterjee PK, Yeboah MM, Dowling O, Xue X, Powell SR, et al. (2012) Nicotinic acetylcholine receptor agonists attenuate septic acute kidney injury in mice by suppressing inflammation and proteasome activity. PLoS One 7: e35361. https://doi.org/10.1371/journal.pone.0035361 PMID: 22586448

86. Wang Y, Sun W, Du B, Miao X, Bai Y, et al. (2013) Therapeutic effect of MG-132 on diabetic cardiomyopathy is associated with its suppression of proteasomal activities: roles of Nrf2 and NF-kappaB. Am J Physiol Heart Circ Physiol 304: H567–578. https://doi.org/10.1152/ajpheart.00650.2012 PMID: 23220333

87. Feng B, Zhang Y, Mu J, Ye Z, Zeng W, et al. (2010) Preventive effect of a proteasome inhibitor on the formation of accelerated atherosclerosis in rabbits with uremia. J Cardiovasc Pharmacol 55: 129–138. https://doi.org/10.1097/FJC.0b013e3181c87f8e PMID: 19935080

88. Dreger H, Westphal K, Wilck N, Baumann G, Stangl V, et al. (2010) Protection of vascular cells from oxidative stress by proteasome inhibition depends on Nrf2. Cardiovasc Res 85: 395–403. https://doi.org/10.1093/cvr/cvp279 PMID: 19679681

89. Zimmermann J, Erdmann D, Lalande I, Grossenbacher R, Noorani M, et al. (2000) Proteasome inhibitor induced gene expression profiles reveal overexpression of transcriptional regulators ATF3, GADD153 and MAD1. Oncogene 19: 2913–2920. https://doi.org/10.1038/sj.onc.1203606 PMID: 10871842

90. Lu J, Murakami M, Verma SC, Cai Q, Haldar S, et al. (2011) Epstein-Barr Virus nuclear antigen 1 (EBNA1) confers resistance to apoptosis in EBV-positive B-lymphoma cells through up-regulation of survivin. Virology 410: 64–75. https://doi.org/10.1016/j.virol.2010.10.029 PMID: 21093004